AD_____

Award Number: DAMD17-99-1-9056

TITLE: Isolation of Motile Tumor Cells from Live Breast Tumors

PRINCIPAL INVESTIGATOR: John Condeelis, Ph.D.

CONTRACTING ORGANIZATION: Albert Einstein College of Medicine
Bronx, New York 10461

REPORT DATE: June 2002

TYPE OF REPORT: Final

PREPARED FOR: U.S. Army Medical Research and Materiel Command
Fort Detrick, Maryland 21702-5012

REPORT DOCUMENTATION PAGE

Form Approved
OMB No. 074-0188

1. AGENCY USE ONLY (Leave blank)	2. REPORT DATE	3. REPORT TYPE AND DATES COVERED
	June 2002	Final (1 Jun 99 - 31 May 02)

4. TITLE AND SUBTITLE
Isolation of Motile Tumor Cells from Live Breast Tumors

5. FUNDING NUMBERS
DAMD17-99-1-9056

6. AUTHOR(S) :
John Condeelis, Ph.D.

7. PERFORMING ORGANIZATION NAME(S) AND ADDRESS(ES)
Albert Einstein College of Medicine
Bronx, New York 10461

E-MAIL:
CONDEELI@AECOM.YU.EDU

8. PERFORMING ORGANIZATION REPORT NUMBER

9. SPONSORING / MONITORING AGENCY NAME(S) AND ADDRESS(ES)
U.S. Army Medical Research and Materiel Command
Fort Detrick, Maryland 21702-5012

10. SPONSORING / MONITORING AGENCY REPORT NUMBER

11. SUPPLEMENTARY NOTES

12a. DISTRIBUTION / AVAILABILITY STATEMENT
Approved for Public Release; Distribution Unlimited

12b. DISTRIBUTION CODE

13. ABSTRACT *(Maximum 200 Words)*

We have developed a method that allows for the direct collection of the invasive population of carcinoma cells from living tumors by taking advantage of the cells inherent ability to chemotax. By filling needles with matrigel and EGF or CSF-1, we are able to collect only the motile population. By using CLontech's SMART technology, we are able to amplify the mRNA from the collected cells to create cDNA usable for microarray analysis. From this, we have discovered important genes in the motility pathways that are differentially expressed. This gene discovery allows for potential new therapeutic targets against breast cancer. Further, we have discovered a paracrine loop that exists between carcinoma cells and macropohages that aids in invasion. This also has implications for new and novel therapeutic targets.

20030502 102

14. SUBJECT TERMS
breast cancer, intravasation, cell collection, intravital imaging

15. NUMBER OF PAGES
29

16. PRICE CODE

17. SECURITY CLASSIFICATION OF REPORT	18. SECURITY CLASSIFICATION OF THIS PAGE	19. SECURITY CLASSIFICATION OF ABSTRACT	20. LIMITATION OF ABSTRACT
Unclassified	Unclassified	Unclassified	Unlimited

Table of Contents

Introduction

Metastasis represents the major cause of mortality in breast cancer patients. Components of the metastatic process can include growth at the primary site, attraction of new blood vessels to the primary tumor, dissemination of tumor cells in the surrounding connective tissue, intravasation and distribution of tumor cells in the blood stream or lymphatics, spread to axillary lymph nodes, extravasation across blood vessel walls and into tissue parenchyma at a secondary site, and growth at the secondary site. These components encompass and rely upon a large number of cellular functions. Cell motility is believed to be important for dissemination of cells from the primary tumor, intravasation, and extravasation. Proof that the motility of tumor cells is a key component in metastasis would be a major advance.

We have developed a collection process that allows for the selective isolation of the motile population of tumor cells from a living breast tumor (1). By using an imaging technique we developed, we have been able to identify the motile cells within a tumor and show that intravasation plays a major role in the dissemination of cells during metastasis (2,3). Further, by comparing differential gene expression based on behavioral differences between non-metastatic and metastatic tumors obtained through our imaging technique, we were able to discover genes important to the motility pathways that were differentially expressed (4). By using a needle filled with matrigel and growth factors as a catheter to mimic a blood vessel, we are able to passively collect motile cells. We have used EGF and CSF-1 to collect both carcinoma cells and macrophages. This has led to discovery of a paracrine loop between these wto cell types that aids in intravasation. We also have been able to amplify the mRNA from the collected cells to further discover gene differences between the invasive population and the primary tumor.

Body

In the originally reported data from the first two reports, we showed that orthotopically injected adenocarcinoma cells could be actively collected using matrigel loaded needles and that when these needles were filled with either EGF or 10% serum that the cells where collected up to 4-5 fold greater in number to around 1000 cells total. By doing these experiments in GFP labeled tumors, using our well characterized cells: MTLn3, a highly metastatic cell line and MTC, a low metastatic cell line (5,6), we were able to visualize invasive motility within the tumor and characterize behavorial differences between the two tumor types (2,3). Multiphoton microscopy has greatly enhanced the quality of the image and due to the second harmonic generation of matrix proteins, we have been able to further characterize extracellular matrix(4).

During the final period of the grant, we have used this behavioral analysis along with microarray analysis to find differentially expressed genes that correlate to behavior. Using multiphoton microscopy, we found 5 major differences in carcinoma cell behavior between the non-metastatic and metastatic primary breast tumors involving extracellular matrix, cell motility and chemotaxis. Behavioral differences were correlated with 7 categories of molecules that were differentially expressed and related to these behaviors. We have found that ECM composition, actin nucleation factors, molecules involved in mechanical stability and survival, and cell polarity and chemotaxis showed large and consistent differences in gene expression. We conclude that aligning cell behavior *in vivo* with patterns of gene expression can lead to new insights into the micro-environment of carcinoma cells in the primary tumor and molecular mechanisms behind cell behavior (4). (see included manuscript)

In further examining the cell collection method we developed, we were able to determine that either EGF or CSF-1 collect both macrophages and carcinoma cells. Immunostaining of collected cells using anti-F/480, a macrophage specific protein, and anti-keratin for carcinoma staining, with DAPI used for all other cell types, we found that approximately 73% of all cells collected were carcinoma cells, 25% macrophages, and all other cell types were less than 1 %. By using PD153035, an EGF receptor tyrosine kinase inhibitor, and blocking antibodies for the CSF-1 receptor, we were able to show that the collection of both cell types requires activity by both receptors. We have concluded that a paracrine loop exists between these two cell types that aids in the intravasasive properties of the metastatic cells. Intrvital imaging using the GFP labeled cells and macrophages phagocytically loaded with Texas-Red Dextran, we were able to visualize these two cell types along vessels in the tumor and that intravasation only occurred where macrophages are present.

Combining the cell collection method with the behavioral analysis and the microarray gene discovery, we have been able to selectively discover genes that are differentially expressed between the invasive cells and the carcinoma cells that make up the tumor. This is done by magnetically removing the macrophages from the cell collected sample and using Clontech's SMART technology to amplify the mRNA to a usable cDNA. Cells from the tumor can be FACS sorted due to their GFP fluorescence. The genes that are differentially expressed between the two populations are put through a supervised selection based on the behavioral analysis reported above.

From this analysis, we have found several important genes that we will continue to study that are important markers for cell motility and intravasation.

In our original application, we reported that we would use laser capture microdissection as a secondary means to collect cells. We found that our collection method was so successful and ultimately selective that we felt it unnecessary to further pursue laser capture microdissection. Laser capture microdissection involves the subjective selection of cells based on their morphology. This means that cells selected may not be invasive but only appear to be in fixed material. Our method uses live material, still in the animal to use chemotaxis to select only the truly invasive cells.

Key Research Accomplishments

- Behavioral analysis based on visualized differences between metastatic and non-metastatic tumors using GFP and multiphoton technologies.
- Gene differences based on differentially expressed genes selected using the Behavioral differences as the basis for selection.
- Chemotactic collection of cells from living tumors using matrigel and EGF, CSF-1 or serum filled needles.
- The discovery of a paracrine loop between carcinoma cells and macrophages using our cell collection technique.
- Gene differences between the invasive population and the whole tumor using cell collected by our method that are possibly important markers for metastasis.

Reportable Outcomes

Manuscripts:

Wyckoff, J. Segall, J., and Condeelis, J. (2000) The collection of the motile population of cells from a living tumor. Canc. Res. 60:5401-5404

Wang, Wyckoff, Frolich et al (2002) Single cell behavior in metastatic primary tumors correlated with gene expression patterns revealed by molecular profiling. Can. Res. 62:6278-6288.

Abstracts:

Wyckoff, J., Frohlich, V., Jones, J., Segall, J. and Condeelis, J. (2000) Imaging of primary tumors in whole animals using laser-based tomography. San Antonio Breast Cancer Symposium.

Wyckoff, J., Bailly, M., Jones, J., Segall, J. and Condeelis, J. (2000)The rate limiting step in metastasis: In vivo analysis of intravasation at the primary tumor.. San Antonio Breast Cancer Symposium.

Wang, W., Wyckoff, J., Zhou, P., Segall, J., and Condeelis, J. (2001) Use of SMART cDNA probe synthesis in array based gene expression profiling to characterize the invasive subpopulation of carcinoma cells in primary tumors. Molecular Targets and Cancer Therapeutics, AACR, Miami, Fl.

Wang, W. Wyckoff, J., Segall, J., and Condeelis, J.(2002)Gene expression Analysis Using cDNA microarrays on small numbers of invasive cells collected from primary tumors. Era of Hope, Dept. of Defense Breast Cancer Research , Orlando, Fl.

Presentations:

Invited seminars by J. Wyckoff, W. Wang, J. Segall, J. Condeelis, J. Pollard at NCI workshops, universities and scientific meetings.

Funding applied for:

NIH/NCI R21/R33 : Novel Imaging Methods for Gene Discovery in Cancer, J. Condeelis P.I., J. Segall co-P.I. (funded)

NIH/NCI P01: Motility and Invasion, J. Condeelis P.I., (submitted)

Conclusions

We have developed a cell collection method that allows for the active and selective collection of the invasive population of cells from living tumors. Using GFP-labeled cells and multiphoton technology, we are directly able to classify behavioral differences between metastatic and non-metastatic tumors and image the collection of the invasive cells. Also, we have discovered a paracrine loop that exists between carcinoma cells and macrophages. On these collected cells, we have performed supervised gene discoveries that shed light on the differentially expressed genes involved in the invasive pathways and that drive the paracrine

loop. These novel methods will hopefully lead to new gene targets for the fight against cancer based on cell motility and cell signaling.

References

1. Wyckoff, J. Segall, J., and Condeelis, J. (2000) The collection of the motile population of cells from a living tumor. Canc. Res. 60:5401-5404

2. Wyckoff, J., Condeelis, J., Jones, J., and Segall, J. (2000) A Critical Step in Metastasis: *In vivo* analysis of intravasation at the primary tumor. Canc. Res. 60:2504-2511.

3. Farina, K. L., Wyckoff, J., Rivera, J., Lee, H., Segall, J. E., Condeelis, J. S., and Jones, J. G. (1998) Cell motility of tumor cells visualized in living intact primary tumors using green fluorescent protein. Canc. Res., 58:2528-2532.

4. Wang, Wyckoff, Frolich et al (2002) Single cell behavior in metastatic primary tumors correlated with gene expression patterns revealed by molecular profiling. Can. Res. 62:6278-6288.

5. Neri, A., Welch, D., Kawaguchi, T., and Nicolson, G. L. (1982) Development and biologic properties of malignant cell sublines and clones of a spontaneously metastasizing rat mammary adenocarcinoma. J. Natl. Cancer Inst. 68:507-517.

6. Edmonds, B.T., Wyckoff, J. Yeung, Y.G., Wang, Y., Stanley, E.R., Jones, J., Segall, J., and Condeelis, J. (1996) Elongation factor-1α is an overexpressed actin binding protein in metastatic rat mammary adenocarcinoma. J. Cell Sci 109:2705-2714.

Bibliography of Publications and Meeting Abstracts

Wyckoff, J. Segall, J., and Condeelis, J. (2000) The collection of the motile population of cells from a living tumor. Canc. Res. 60:5401-5404

Wang, Wyckoff, Frolich et al (2002) Single cell behavior in metastatic primary tumors correlated with gene expression patterns revealed by molecular profiling. Can. Res. 62:6278-6288.

Abstracts:

Wyckoff, J., Frohlich, V., Jones, J., Segall, J. and Condeelis, J. (2000) Imaging of primary tumors in whole animals using laser-based tomography. San Antonio Breast Cancer Symposium.

Wyckoff, J., Bailly, M., Jones, J., Segall, J. and Condeelis, J. (2000)The rate limiting step in metastasis: In vivo analysis of intravasation at the primary tumor.. San Antonio Breast Cancer Symposium.

Wang, W., Wyckoff, J., Zhou, P., Segall, J., and Condeelis, J. (2001) Use of SMART cDNA probe synthesis in array based gene expression profiling to characterize the invasive subpopulation of carcinoma cells in primary tumors. Molecular Targets and Cancer Therapeutics, AACR, Miami, Fl.

Wang, W. Wyckoff, J., Segall, J., and Condeelis, J.(2002)Gene expression Analysis Using cDNA microarrays on small numbers of invasive cells collected from primary tumors. Era of Hope, Dept. of Defense Breast Cancer Research , Orlando, Fl.

List of Personnel funded by this grant

John Condeelis, P.I.
Jeff Wyckoff, Faculty Assoc

The Rate-Limiting Step in Metastasis: In Vivo Analysis of Intravasation at the Primary Tumor.

Wyckoff JB, Bailly M, Jones JG, Condeelis JS, Segall JE. Anatomy and Structural Biology Pathology, Albert Einstein College of Medicine, Bronx, NY.

Determination of the rate-limiting step in tumor cell metastasis is critical for evaluating the cell mechanisms controlling metastasis. Using GFP transfectants of the metastatic MTLn3 and non-metastatic MTC cell lines derived from the rat mammary adenocarcinoma 13762 NF, we have measured tumor cell density in the blood, individual cells in the lungs, and lung metastasis. Correlation of blood burden with lung metastases indicates that entry into the circulation is a rate-limiting step for metastasis for both metastatic and non-metastatic cell lines. Consistent with previous work, cell arrest in the lungs is efficient, while growth of metastases in the lungs is inefficient. To examine cell behavior at the critical step of intravasation, we have used GFP technology to view these cells in time lapse images within a single optical section using a confocal microscope (see abstract by Condeelis et al.). In vivo imaging of the primary tumors of MTLn3 and MTC cells indicates that both metastatic and non-metastatic cells are motile and shoe protrusive activity. However, metastatic cells show greater orientation towards blood vessels, and larger numbers of host cells within the primary tumor, while non-metastatic cells show greater fragmentation. Metastatic cells show chemotactic responses to EGF in vitro, and such responses in vivo may enable metastatic cells to avoid fragmentation and thus enhance their ability to survive entry into the circulation. These results demonstrate that cell-based assays for determination of cell properties in vivo are necessary for dissection of the metastatic process.

Imaging of Primary Tumors in Whole Animals Using Laser-Based Tomography.

Wyckoff JB, Frohlich V, Jones JG, Segall JE, Condeelis JS. Anatomy and Structural Biology Pathology, Albert Einstein College of Medicine, Bronx, NY; Optical Imaging Center, University of Texas Health Science Center, San Antonio, TX.

We have developed a model in which the motility, adhesion and cell-cell interactions can be examined in live primary tumors in whole animals. Subcutaneous injection of GFP-expressing cells with graded metastatic potential into the mammary fat pad of female Fischer 344 rats generates primary tumors that fluoresce when GFP excited. Moving cells are imaged in the live rats under anesthesia, with either a laser scanning confocal or a multiphoton microscope. Imaging at high resolution in the non-metastatic and metastatic tumors demonstrates significant differences between the two which account for differences in metastatic potential (see abstract by Segall et al.). Non-metastatic tumors are more fibrous and less necrotic with tumor cells that are highly polarized and less motile. Metastatic tumors are more necrotic with tumor cells that are unpolarized except near blood vessels where they are highly polarized with cell protrusions toward the vessel. Metastatic cells move in groups or streams of cells suggesting a preferred micro-environment for locomotion and probable chemotaxis in vivo. Comparison of imaging with the laser scanning confocal and multiphoton microscopes demonstrates the greater imaging depth of the multiphoton microscope (~10x) in these breast tumors. This allows direct and rapid observations of the blood vessel distribution in primary tumors. Multiphoton imaging also permits visualization of extracellular matrix directly due to its autofluorescence in the near UV allowing the observation of cell adhesion and proteolysis in vivo and its correlation with cell motility. This is the first model that allows direct observations of metastasis in an intact orthotopically grown primary tumor while in the live animal.

.

Use of SMART cDNA probe synthesis in array based gene expression profiling to characterize the invasive subpopulation of carcinoma cells in primary tumors.

W. Wang, J.B. Wyckoff, P. Zhou, J. E. Segall, J. S. Condeelis. Albert Einstein College of Medicine, Bronx, NY.

We have developed metastasis models in rats and mice that are clinically relevant in that they resemble human breast tumors in etiology and histology, permitting real time multiphoton-based imaging of the behavior and interactions of metastatic tumor cells in the primary tumor in vivo. Our previous work has demonstrated that needles filled with growth factors and Matrigel, when inserted into the primary tumor, can faithfully mimic the environment that supports invasion and intravasation in vivo. The most efficient cell collection requires the presence of chemotactic cytokines such as EGF and serum components and occurs with 15 fold higher efficiency in metastatic tumors compared to non-metastatic tumors. This indicates that additional factors besides random cell motility are required to explain differences in cell collection efficiencies between metastatic and non-metastatic tumors. Recently, large scale nucleic acid arrays have become very useful tool to investigators exploring differences in gene expression between cell types, stages of differentiation, or cellular responses to stimuli and changes in environment. The fusion of chemotaxis based cell collection with array based gene expression analysis has the potential to identify the genes necessary for individual steps of invasion at the cellular level, and for the rational interpretation of gene expression patters in metastatic tumors. One drawback to the array technique is the need to isolate and purify microgram amounts of poly(A)+ RNA or around 100 microgram total RNA to generate the appropriate probe. In our study, the amount of available cells is very limited. Typically, needle collection yields about 1,000 cells containing 30-50 ng of total RNA, well below the amounts needed for arrays. In this study, to validate the use of PCR-amplified full-length cDNA for array based gene expression analysis, SMART cDNA synthesis technology (Clontech) was used. Full-length cDNA generated from the RNA pool from 1,000 cells was PCR amplified, and then the amplified cDNA was used as a hybridization probe. As quantitated by real time PCR, the relative abundance of genes is maintained during the SMART PCR amplification. We compared the expression profile of 9,000 genes for the total RNA method to that obtained with SMART PCR probe. The results from triplicate experiments showed that SMART cDNA probe yields gene expression profiles that represent the majority of transcripts detected with conventional methods. By further comparing the gene expression patterns of cells collected by invasion into needles with that of cells obtained from the whole primary tumor, the blood, and whole metastatic tumors, genes that contribute to the invasive process uniquely may be identified.

Gene Expression Analysis Usinn cDNA Microarrays on Small Numbers of Chemotactic Cells Collected From Primary Tumors.

Weigang Wang, Jeffreey B. Wyckoff, Jeffrey E. Segall and John S. Condeelis

We have developed metastasis models in rats that are clinically relevant in that they resemble human breast tumors in etiology and histology, permitting real time multiphoton-based imaging of the behavior and interactions of metastatic tumor cells in the primary tumor in vivo. Our previous work has demonstrated that microneedles filled with growth factors and Matrigel, when inserted into the primary tumor, can faithfully mimic the environment that supports invasion and intravasation in vivo. The most efficient cell collection requires the presence of chemotactic cytokines such as EGF and serum components and occues with 15-fold higher efficiency in metastatic tumors compared to non-metastatic tumors. We have been able to refine the methods necessary for collectinf invasive cells from the primary tumor and we can characterize the collection process by direct intravital imaging using the multiphoton microscope. We have been able to position the microneedles in random areas of the tumor allowing a survey of different microenviroments within the tumor. The experimental approach has allowed us to obtain evidence for a paracrine interaction between carcinoma cells and macrophages that increases the invasive potential of the carcinoma cells and the metastatic potential of the tumors.

The fusion of the chemotaxis based cell collection with array based gene expression analysis has the potential to identify the genes necessary for individual steps of invasion at the cellular level, and for the rational interpretation of gene expression patterns in metastatic tumors. One drawback to the array technique is the need to isolate and purify microgram amounts of poly(A)+ RNA or around 100 micrograms total RNA to generate the appropriate probe. In our study, microneelde collection yields about 1,000 cells containing 30-50 ng of total RNA, well below the amounts needed for arrays. In this study, to validate the use of PCR-amplified full length cDNA for array based gene expression analysis, SMART cDNA synthesis technology (Clontech) was used. Key to this alternative approach is the reproducible and representative synthesis of cDNA probes that retain faithfully the complexity of the mRNA population present in the original sample. We compared two approaches for synthesizing cDNA probes from total RNA for use with subsequent hybridization to high density cDNA microarrays: 1) the conventional approach of reverse transcription (RT) of 100 ug of total RNA from cultures of carcinoma cells, and 2) RT-PCR of ~30ng ot total RNA from 1000 carcinoma cells using the SMART system. The results demonstrate that, for situations of limited RNA, the SMART probe synthesis method retains the original mRNA message profile, and is suitable for gene expression profiling of invasive cells collected in microneedles. This technology will allow the characterization of gene expression patterns of tumor cells within the primary tumor during invasion and in response to varying genetic backgrounds. It will also make possible the identification of paracrine and other microenviroment-dependent interactions that contribute to the invasive process.

[CANCER RESEARCH 60, 5401–5404, October 1, 2000]

Advances in Brief

The Collection of the Motile Population of Cells from a Living Tumor

Jeffrey B. Wyckoff, Jeffrey E. Segall, and John S. Condeelis[1]

Departments of Anatomy and Structural Biology, Albert Einstein College of Medicine, Bronx, New York 10461

Abstract

In this study, we report that needles containing chemoattractants can be used to collect the subpopulation of motile and chemotactic tumor cells from a primary tumor in a live rat as a pure population suitable for further analysis. The most efficient cell collection requires the presence of chemotactic cytokines, such as epidermal growth factor and serum components, and occurs with 15-fold higher efficiency in metastatic tumors compared with nonmetastatic tumors. Although tumor cells of the nonmetastatic tumors show a motility response to serum, they were not collected with high efficiency into needles *in vivo* in response to serum, indicating that additional factors besides motility are required to explain differences in cell collection efficiencies between metastatic and nonmetastatic tumors. The results reported here indicate that needles filled with growth factors and matrigel, when inserted into the primary tumor, can faithfully mimic the environment that supports invasion and intravasation *in vivo*. Furthermore, the results indicate that the same cell behaviors that contribute to chemotaxis *in vitro* also contribute to invasion *in vivo*.

Introduction

Metastasis involves the escape of cells from the primary tumor either via lymphatics or blood vessels, transport to and arrest in a target organ, and growth of metastasis in the target organ (1). Each of these steps is a multicomponent process, with potentially different tumor cell properties and molecules playing critical roles at different steps (2). Recently, emphasis has been on the development of molecular arrays to identify new genes and proteins that contribute to specific steps in metastasis. Such approaches are crucial in the analysis of cancer as a genetic disease and in the identification of key genes that might be used in diagnosis and therapy. However, array-based approaches treat the tumor as a black box. Ideally, high-resolution methods for the analysis of metastasis at the cellular level, such as imaging of cells within tumors, when combined with array-based approaches, could be used to accurately evaluate the roles of specific gene products in the individual steps of metastasis at the cellular level. The use of Laser Capture Microdissection as a front end for array-based gene discovery is such a fusion approach (3). However, some of the cell behaviors that are believed to be essential for metastasis, such as adhesion and motility (4, 5), cannot be used as criteria in the selection of cells for analysis from fixed material because the behavior and history of individual cells cannot be inferred from fixed material. Methods for the collection of cells from living tumors in which key cell behaviors can be observed and used as the criteria for cell collection need to be developed. One such cell behavior is the chemotaxis of tumor cells. Metastatic tumor cells are believed to chemotax to cytokines that are normally found in association with blood vessels (6–8). We developed a cell graft breast tumor metastasis model in rats that is syngeneic and orthotopic that permits the imaging and tracking of cell behavior in live tumors (8, 9). Using this model, we have observed, in metastatic primary tumors, the highly persistent linear locomotion of a subpopulation of tumor cells toward blood vessels *in vivo* using intravital imaging. This locomotion resembles the chemataxis of cells observed in culture (9, 10) and is correlated with metastatic potential (10, 11). Tumor cell chemotaxis is also correlated with the accumulation of metastatic tumor cells around, and their polarization toward, blood vessels in the primary tumor. Furthermore, chemotaxis is correlated with the efficient intravasation into, and survival of tumor cells in, the systemic circulation (8). Because these properties are not observed in nonmetastatic tumors prepared from cells in the same way (7, 8), polarization and chemotaxis toward blood vessels are believed to be important in intravasation and metastasis (8). In this study, we report that chemotaxis can be used to advantage to collect the subpopulation of motile and chemotactic tumor cells from a primary tumor *in vivo* as a pure population suitable for further analysis.

Materials and Methods

Serum Upshift of Cells *in Vitro*. MTLn3-GFP and MTC-GFP cells were plated in 35-mm dishes at a density of 50,000 cells per dish 18 h before the experiment. On the day of the experiment, cells were starved for 3 h in 2 ml of MEM containing HEPES and 0.69% BSA, which is the isotonic equivalent of 10% FBS[2]. The upshift was performed as described before (12), with the exception that the cells were stimulated with 10% FBS. Briefly, the dishes were covered with a thin layer of heavy mineral oil (Sigma #400-5) and placed in an enclosed microscope preheated to 37°C. Using a CCD camera, single-frame images were collected using NIH Image every minute. After 4 min, 2 ml of MEM with HEPES and 20% FBS were added to the dish, and image frames were collected for an additional 16 min.

***In Vitro* Cell Collection.** MTLn3 cells were plated in a 35-mm dish 18 h before the experiment to be 60–80% confluent at the time of the experiment. On the day of the experiment, cells were starved using MEM-BSA, the isotonic equivalent of 5% FBS, for 2 h. During this time, 26-gauge syringe needles were prepared by filling them with 10 μl of Matrigel mixed 1:1 with MEM-BSA or MEM-BSA containing EGF for a final concentration of 0.5 nM, 2.5 nM, 5 nM, 25 nM, 50 nM, or 250 nM EGF. After starvation, the needles were attached to the side of the plate using paraffin to hold them in place with the bevel of the needle facing the bottom of the plate so that the matrigel was in contact with the surface of the plate. Dishes were placed into a 37°C/5.0% CO_2 incubator for up to 6 h. After this time, the contents of each needle was extruded into a new 35-mm dish containing MEM with 5% FBS (growth medium). Cells that had entered the needle were allowed to grow into clones for 6 days to determine cell count and viability. Positive clones, checked by GFP fluorescence and cell morphology, were then counted.

To image the cells moving toward the needle, a dish was plated for 40–50% confluency before the experiment. Cells were starved, and a needle was prepared as above containing matrigel mixed 1:1 with MEM-BSA containing 25 nM EGF. Images as single frames were taken using the heated microscope and NIH Image every 30 min, as described above. The dish was kept in a 37°C/5% CO_2 incubator between images.

***In Vivo* Cell Collection.** MTLn3-GFP and MTC-GFP cells were injected into female Fischer 344 rats, as described before (8, 9), and tumors were

Received 4/19/00; accepted 8/16/00.

The costs of publication of this article were defrayed in part by the payment of page charges. This article must therefore be hereby marked *advertisement* in accordance with 18 U.S.C. Section 1734 solely to indicate this fact.

[1] To whom requests for reprints should be addressed, at Departments of Anatomy and Structural Biology, Albert Einstein College of Medicine, 1300, Morris Park Avenue, Bronx, NY 10461. Phone: (718) 430-4068; Fax: (718) 430-8996; E-mail: condeeli@aecom.yu.edu.

[2] The abbreviations used are: FBS, fetal bovine serum; MEM-BSA, MEM with 0.35% BSA; EGF, epidermal growth factor; i.d., inside diameter; GFP, green fluorescent protein.

allowed to grow for 2.5 weeks. On the day of the experiment, 33-gauge needles were prepared as above by filling them with matrigel and MEM-BSA, MEM-BSA with a final EGF concentration of 25 nM, or MEM-BSA with a final FBS concentration of 10%. All needles included 0.01 mM EDTA (pH 7.4) to sequester heavy metals that might be released by the needle. A rat was anesthetized using 5% isoflurane and laid on its back. The isoflurane was reduced to 2%, and a small patch of skin over the tumor was removed. Three 25-gauge needles (guide needles) with blocking wires were inserted to a depth of 2 mm. The blocking wire was removed, and one of the matrigel-filled needles was inserted into each guide needle (as shown in Fig. 3). The needle was then left in the tumor for 6 h. The isoflurane concentration was slowly lowered to 0.5% during the course of the experiment to keep the rat's breathing even and unlabored. After 6 h, the needles were withdrawn, extruded into 35-mm dishes containing growth medium, and all cells were counted immediately. The percentage of cells with GFP fluorescence was determined.

As a control for the effects of matrigel, a 33-gauge needle was filled as above with MEM-BSA and agarose, for a final concentration of 1%, and the *in vivo* experiment was performed as above.

Results

***In Vitro* Cell Collection.** As has been shown previously, MTLn3 cells are chemotactic to EGF with an optimum concentration at 5 nM EGF (12). Also, it has been shown that MTLn3 cells, when placed in a gradient generated using a pipette filled with 50 μM EGF, will orient toward and locomote in the direction of the pipette exhibiting true amoeboid chemotaxis (10). MTLn3 cells are metastatic when reinjected into the mammary fat pad of a Fischer 344 rat. We prepared an artificial microenvironment using microneedles filled with matrigel and either EGF or serum as the chemoattractant to simulate invasion and intravasation into a container that could be withdrawn to collect the chemotactic/invasive subpopulation of cells.

To establish the concentration necessary to attract MTLn3 cells into the needle, needles were filled with a range of EGF concentrations from 0.5–250 nM and inserted into a cell culture. At times up to 6 h of collection, the needles were withdrawn from the culture and the contents were extruded into a new dish with growth medium, and the cells were allowed to grow for 6–7 days to determine cell counts and test viability. The number of cells entering the needle was determined by the number of GFP fluorescent clones that grew during this time. At the peak concentration of 25 nM EGF, an 8-fold increase in the number of cells entering the needle was seen, when compared with buffer alone (Fig. 1). The number of cells collected decreased at 50 nM EGF, and by 250 nM EGF the number of cells collected returned to near background.

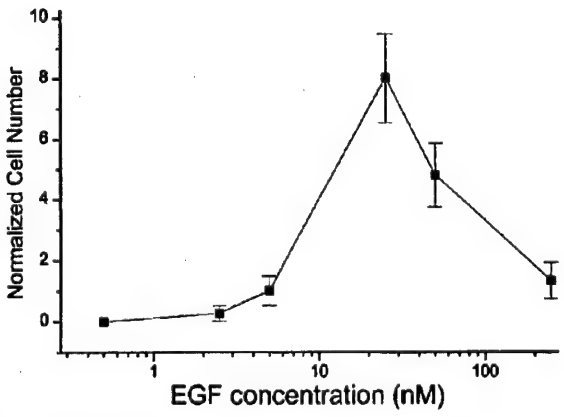

Fig. 1. Tumor cells are collected into matrigel-containing needles in response to EGF. Cells in culture were collected in needles containing matrigel and differing concentrations of EGF. The maximal number of cells was collected into the needle containing 25 nM EGF. Cell numbers were normalized to MTLn3 cells collected with matrigel in buffer. *Bars*, the SE of three experiments.

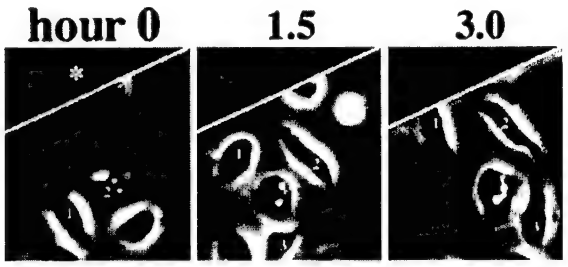

Fig. 2. Tumor cells chemotax toward needles containing EGF. Cells are seen orienting and moving toward a needle containing matrigel and 25 nM EGF. By 1.5 h after the needle was placed in the culture dish, cells 1 and 2 have already oriented themselves toward and have moved in the direction of the needle, whereas cell 3 has entered the field of view. By 3 h, cells 1 and 2 have reached the matrigel edge. The edge of the matrigel (*) is delineated by the *white line* and shown in *gray*. Only motile cells within the field are numbered. The average velocity of the cells is 0.32 ± 0.03 μm/min.

The differences in EGF concentration optimum for cell response between the upshift (5 nM; Ref. 12), the pipette experiment (50 μM; Ref. 10), and the collection experiment reported here (25 nM) can be explained by the differences in diffusion of EGF in the different experimental designs. In the upshift, there is no gradient involved and the cells see an equal and constant concentration of EGF. For the pipette experiment the gradient is created by a pipette with an i.d. of <1 μm, and the concentration outside of the pipette is only a fraction of the concentration in the pipette. For the *in vitro* cell collection experiments reported here the i.d. of a 26-gauge needle is 250 μm; hence, a larger percentage of EGF is delivered per unit time so that a much lower EGF concentration is necessary than in the pipette experiment (10).

By using a needle loaded with matrigel and 25 nM EGF in MEM-BSA, we were able to capture images of the cells moving toward the pipette, using time-lapse video-microscopy. In Fig. 2, the matrigel surface at the edge of the needle is delineated by the *white line* and colored *gray*. At time zero, cells 1 and 2 are seen as nonpolarized cells with no discernable leading edge. After 1.5 h, cells 1 and 2 have oriented themselves toward and moved in the direction of the needle-induced EGF gradient, extending a leading lamellapod toward the needle. Cell 3 has also moved into the field. After 3 h, all three cells can be seen to have moved measurably closer to the needle. The cells move toward the needle at a velocity of 0.32 μm/min, which is comparable with the velocities reported previously (10).

***In Vivo* Cell Collection.** To determine whether cells can be collected from tumors *in vivo* and, if so, if there is a difference in collection efficiency of cells from nonmetastatic and metastatic tumors, experiments were performed by placing needles into the primary tumors generated by either the nonmetastatic MTC-GFP or the metastatic MTLn3-GFP cell lines. For this, a 33-gauge needle (i.d., 102 μm) was filled as above and inserted into the guide syringe after a blocking wire was removed (as modeled in Fig. 3). The needles were filled with matrigel plus either buffer, 25 nM EGF, or 10% FBS. The 10% FBS was used because the motility of both MTLn3 and MTC cells is stimulated in response to 10% serum (data not shown). After 6 h of collection, needles were withdrawn and the contents of each was extruded into a 35-mm dish containing growth medium, and collected tumor cells were determined by GFP fluorescence. To confirm that only GFP-labeled cells were in the needle, 1 μg/ml DAPI (4′,6-diamidino-2-phenylindole) was added to the dish to stain all cells. All DAPI-stained nuclei were in GFP-labeled cells, indicating that only tumor cells were collected.

The number of cells collected for each condition was normalized to the number of cells collected from the MTC-GFP tumors using needles containing matrigel plus buffer (MEM-BSA) only (Fig. 4).

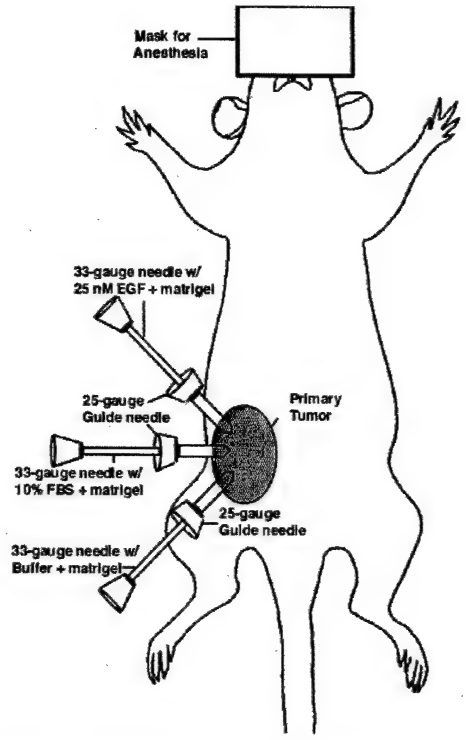

Fig. 3. Method for using needles for *in vivo* cell collection. Needles (i.d., 102 μm) filled with matrigel and buffer, 25 nM EGF, or 10% FBS are shown placed in 25-gauge guide needles that are inserted into the primary tumor of an anesthetized rat.

For the needle with 25 nM EGF, 15.3 times more MTLn3 cells were collected from metastatic MTLn3 tumors compared with MTC cells from nonmetastatic MTC tumors under the same conditions of collection. In this case, a maximum of 100 cells was collected. Needles containing 10% FBS showed only a 6.0-fold difference between the two tumor types under the same conditions (Fig. 4). There was a 2-fold increase in the number of MTC cells entering the 10% FBS needle from the MTC tumors compared with the number of cells that entered the needle containing only buffer. This difference was shown to be significant (t test value, 0.027) and is consistent with the increase in motility of MTC cells when stimulated with 10% FBS *in vitro* (data not shown). We did not attempt to establish long-term cultures of tumor cells collected from the tumors *in vivo* under any of these conditions.

In addition, in needles containing only buffer, 4.3 times more tumor cells were collected from MTLn3 tumors than from MTC tumors (Fig. 4). To determine whether this was due to a cell response to matrigel, a needle was filled with either 1% agarose containing MEM-BSA or 1% agarose containing 10% FBS in MEM-BSA. MTLn3 cells are able to adhere and grow on agarose. However, agarose was chosen because it is a polysaccharide that cannot be degraded by proteases. The number of cells entering the agarose needles was at background for both the 10% FBS-containing needle (data not shown) and the needle with buffer alone (Fig. 4), indicating that either components within the matrigel or the degradation of matrigel provides a chemotactic signal to the cells.

The collection of cells from the MTln3 tumors was maximal with needles containing 25 nM EGF, resulting in the collection of about 100 cells in 6 h. Because the diameter of the 33-gauge collecting needle is 100 um and the average cell diameter is 25 um, the calculated average velocity of cell motility required to account for the collection of 100 cells in 6 h is 0.3 um/min. This value is very close to the velocity of cell locomotion observed *in vitro* during chemotaxis (Fig. 2).

Discussion

In this study, we report that needles containing chemoattractants can be used to collect the subpopulation of motile and chemotactic tumor cells from a primary tumor *in vivo* as a pure population suitable for further analysis. Our results demonstrate that tumor cells are collected into needles that have been inserted into a primary tumor when they contain either serum, EGF, or matrigel but not agarose, indicating that a tactic signal is required for collection. The most dramatic accumulation of cells in the needles occurs in response to either EGF or serum. EGF is known to be a chemoattractant for MTLn3 cells (10), whereas serum stimulates the motility of both MTLn3 and MTC cells. However, matrigel was sufficient to collect cells above background, indicating that either the matrigel contains cytokines that are chemotactic for these cells or that limited proteolysis resulting from the interaction of the matrigel with the tumor is sufficient to generate a gradient of chemotactic peptides. Either possibility is consistent with the known properties of matrigel (13–15). Furthermore, MTLn3 cells have a 4-fold greater activity compared with MTC cells (16), which may explain the increase in the number of MTLn3 cells collected into the needles containing matrigel compared with that for MTC cells.

Both EGF and transforming growth factor α are growth factors found in mammary tissue. MTLn3 cells have around 50,000 EGF receptors/cell, whereas EGF receptors on the MTC cells are not detectable (9). By using EGF as the chemoattractant, we were able to selectively collect 15 times as many metastatic MTLn3 cells from MTLn3-derived metastatic primary tumors as MTC cells from MTC-derived nonmetastatic tumors. Serum, which contains many growth factors with potential chemotactic activity, also stimulated the collection of tumor cells from MTLn3 tumors. Although MTC cells show a motility response to serum, they were not collected with high efficiency into needles in response to serum, indicating that additional factors besides motility are required for the large increase in the number of MTLn3 cells collected in response to serum.

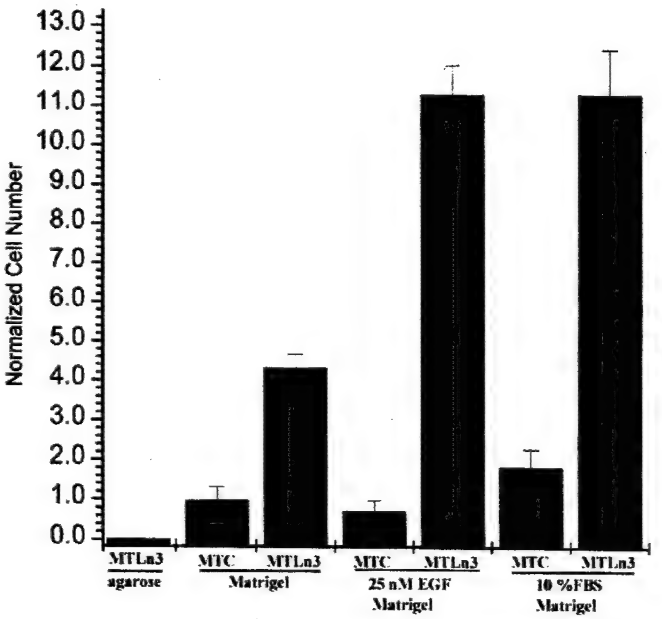

Fig. 4. Metastatic cells (MTLn3) are more efficient than nonmetastatic cells (MTC) at entering matrigel-filled needles in response to EGF *in vivo*. Cells were collected from metastatic (MTLn3) and nonmetastatic (MTC) tumors using the *in vivo* experiment shown in Fig. 3. The maximum response was for cells from the metastatic MTLn3 tumors into EGF- and serum-containing needles. Cells were collected above background from metastatic tumors in response to matrigel in buffer but not agarose. All counts were normalized to MTC cells collected with matrigel in buffer. *Bars*, the SE of four experiments.

Morphologically, MTC cells are elongated and polarized both *in vivo* and *in vitro*, whereas the MTLn3 cells are generally unpolarized both in culture and in the primary tumor (8, 11). This difference is most dramatically illustrated by using intravital imaging techniques where GFP-expressing tumor cells are imaged directly in the primary tumor (8, 9). *In vivo*, MTLn3 cells are highly polarized around and oriented toward the blood vessels running through the primary tumor. MTC cells, on the other hand, are polarized throughout the tumor, but the polarity is randomly oriented relative to vessels (8, 11).

Characterization of the cells *in vitro* confirms the differences between the two cell lines. In cultures that have not been stimulated with a chemoattractant, MTC cells locomote in a linear direction at approximately twice the velocity of MTLn3 cells. MTLn3 cells, under these conditions, are unpolarized and move in random directions or not at all (11). On stimulation with an EGF gradient, the MTLn3 cells become polarized and move linearly at approximately the same speed as the MTC cells, yet have the ability to reorient themselves to follow an EGF gradient with precision (10), a property not seen in MTC cells.

In vivo, in the primary tumor, both cell types move linearly at approximately the same speeds, but the MTLn3 cells tend to move only when they are polarized and in association with a vessel, whereas MTC cells can be seen moving throughout the tumor (8, 9). The ability of the MTLn3 cells to invade into a needle filled with matrigel in response to growth factors is fully consistent with the chemotactic motility exhibited by these cells *in vitro*, their polarity and locomotion toward vessels *in vivo*, and with the dramatically increased efficiency of intravasation measured as blood burden of tumor cells *in vivo* (8). This suggests that chemotaxis may be the key aspect of cell motility that contributes to invasion and intravasation. It also suggests that needles filled with growth factors and matrigel, when inserted into the primary tumor, can faithfully mimic the environment that supports invasion and intravasation *in vivo,* and that the same cell behaviors that contribute to chemotaxis *in vitro* also contribute to invasion *in vivo*.

An advantage of using the needle collection technique described here for the collection of cells for genomic/proteomic analysis is that the cell behavior can be characterized during the collection process. This can be done by varying the conditions required for cell collection such as the extracellular matrix composition and/or cytokines used as chemoattractants, determining how these changes affect efficiency of cell collection, and then relating these observations to the gene expression and protein composition patterns subsequently obtained from array analysis of the collected cells. Furthermore, cells can also be characterized by intravital imaging during collection to directly visualize the cell-cell and cell-extracellular matrix interactions that contribute to the invasion of the needle under these different conditions. In addition, cells could be cultured and transplanted into other host animals to determine whether they stably retain differential characteristics that contribute to metastatic potential. Finally, by comparing the gene expression patterns of cells collected by invasion into needles with that of cells obtained from the whole primary tumor, the blood, and whole metastatic tumors, genes that contribute to the invasive process uniquely may be identified.

References

1. Fidler, I. J. Critical determinants of cancer metastasis: rationale for therapy. Cancer Chemother. Pharmacol., *43*(Suppl): S3–S10, 1999.
2. Price, J. T., Bonovich, M. T., and Kohn, E. C. The biochemistry of cancer dissemination. Crit. Rev. Biochem. Mol. Biol., *32:* 175–253, 1997.
3. Bonner, R. F., Emmert-Buck, M., Cole, K., Pohida, T., Chuaqui, R., Goldstein, S., and Liotta, L. A. Laser capture microdissection: molecular analysis of tissue. Science (Washington DC), *278:* 1481–1483, 1997.
4. Morris, V. L., Schmidt, E. E., MacDonald, I. C., Groom, A. C., and Chambers, A. F. Sequential steps in hematogenous metastasis of cancer cells studied by *in vivo* videomicroscopy. Invasion Metastasis, *17:* 281–296, 1997.
5. Naumov, G. N., Wilson, S. M., MacDonald, I. C., Schmidt, E. E., Morris, V. L., Groom, A. C., Hoffman, R. M., and Chambers, A. F. Cellular expression of green fluorescent protein, coupled with high-resolution *in vivo* videomicroscopy, to monitor steps in tumor metastasis. J. Cell Sci., *112:* 1835–1842, 1999.
6. Stetler-Stevenson, W. G., Aznavoorian, S., and Liotta, L. A. Tumor cell interactions with the extracellular matrix during invasion and metastasis. Ann. Rev. Cell Biol., *9:* 541–574, 1993.
7. Kaufmann, A. M., Khazaie, K., Wiedemuth, M., Rohde-Schulz, B., Ullrich, A., Schirrmacher, V., and Lichtner, R. B. Expression of epidermal growth factor receptor correlates with metastatic potential of 13762NF rat mammary adenocarcinoma cells. Int. J. Oncol., *4:* 1149–1155, 1995.
8. Wyckoff, J., Jones, J., Condeelis, J., and Segall, J. A critical step in metastasis. *In vivo* analysis of intravasation at the primary tumor. Cancer Res., *60:* 2504–2511, 2000.
9. Farina, K. L., Wyckoff, J., Rivera, J., Lee, H., Segall, J. E., Condeelis, J. S., and Jones, J. G. Cell motility of tumor cells visualized in living intact primary tumors using green fluorescent protein. Cancer Res., *58:* 2528–2532, 1998.
10. Bailly, M., Yan, L., Whitesides, G., Condeelis, J., and Segall, J. Regulation of protrusion shape and adhesion to a substratum during chemotactic responses of mammalian carcinoma cells. Exp. Cell Res., *241:* 285–299, 1998.
11. Shestakova, E., Wyckoff, J., Jones, J., Singer, R., and Condeelis, J. Correlation of β-actin messenger RNA localization with metastatic potential in rat adenocarcinoma cell lines. Cancer Res., *59:* 1202–1205, 1999.
12. Segall, J. E., Tyerech, S., Boselli, L., Masseling, S., Helft, J., Chan, A., Jones, J., and Condeelis, J. EGF stimulates lamellipod extension in metastatic mammary adenocarcinoma cells by an actin-dependent mechanism. Clin. Exp. Metastasis, *14:* 61–72, 1996.
13. Yamamura, K., Kibbey, M. C., Jun, S. H., and Kleinman, H. K. Effect of matrigel and laminin peptide YIGSR on tumor growth and metastasis. Semin. Cancer Biol., *4:* 259–265, 1993.
14. Kibbey, M. C., Grant, D. S., and Klienman, H. K. Role of the SIKVAV site of laminin in promotion of angiogenisis and tumor growth: an *in vivo* matrigel model. J. Natl. Cancer Inst., *84:* 1633–1638, 1992.
15. McGuire, P. G., and Seeds, M. W. The interaction of plaminogen activator with a reconstituted basement membrane matrix and extracellular macromolecules produced by cultured epithelial cells. J. Cell. Biochem., *40:* 215–227, 1989.
16. Nakajima, M., Welch, D. R., Belloni, P. N., and Nicolson, G. L. Degradation of basement membrane type IV collagen and lung subendothelial matrix by rat mammary adenocarcinoma cell clones of differing metastatic potentials. Cancer Res., *47:* 4869–4876, 1987.

[CANCER RESEARCH 62, 6278–6288, November 1, 2002]

Single Cell Behavior in Metastatic Primary Mammary Tumors Correlated with Gene Expression Patterns Revealed by Molecular Profiling[1,2]

Weigang Wang,[3] Jeffrey B. Wyckoff,[3] Victoria Centonze Frohlich, Yuri Oleynikov, Stefan Hüttelmaier, Jiri Zavadil, Lukas Cermak, Erwin P. Bottinger, Robert H. Singer, John G. White, Jeffrey E. Segall, and John S. Condeelis[4]

Departments of Anatomy and Structural Biology [W. W., J. B. W., Y. O., S. H., R. H. S., J. E. S., J. S. C.] and Medicine [J. Z., L. C., E. P. B.], Albert Einstein College of Medicine, Bronx, New York 10461; Department of Cellular and Structural Biology, University of Texas Health Science Center at San Antonio, San Antonio, Texas 78229 [V. C. F.]; and Department of Anatomy, University of Wisconsin-Madison, 1525 INDEN DR, Madison, Wisconsin 53706 [J. G. W.]

ABSTRACT

We have developed animal models of breast cancer that allow the direct examination of the behavior of individual green fluorescent protein-expressing carcinoma cells in live nonmetastatic and metastatic primary tumors *in situ*. We have combined this model with multiphoton microscopy to image differences in cell behavior within the primary tumor. Differences in cell behavior between nonmetastatic and metastatic cells in culture and within live primary tumors were correlated with results from cDNA microarray analyses to identify potentially important genetic determinants for breast cancer invasion and metastasis. Using multiphoton microscopy, we found five major differences in carcinoma cell behavior between the nonmetastatic and metastatic primary breast tumors involving extracellular matrix, cell motility, and chemotaxis. Behavioral differences were correlated with seven categories of molecules that were differentially expressed and related to these behaviors. We have found that extracellular matrix composition, actin nucleation factors, molecules involved in mechanical stability and survival, and cell polarity and chemotaxis showed large and consistent differences in gene expression. We conclude that aligning cell behavior *in vivo* with patterns of gene expression can lead to new insights into the microenvironment of carcinoma cells in the primary tumor and the molecular mechanisms behind cell behavior.

INTRODUCTION

Metastasis is believed to involve the escape of carcinoma cells from the primary tumor via lymphatics and blood vessels, transport to and arrest in a target organ, and growth of metastases in the target organ (1). Each of these steps is a multicomponent process, with families of molecules playing critical roles at different steps. Much work has gone into characterizing metastasis at the late steps from extravasation onward using experimental metastasis, in which carcinoma cells are injected into the circulation of host animals (2, 3). This has led to insights into the adhesion, proteolysis, and proliferation mechanisms that cause metastatic tumors. However, the primary tumor has remained a black box at the single-cell level.

The development of high-density molecular arrays has led to the identification of new genes and proteins that contribute to specific steps in metastasis within the primary tumor (4, 5). Such approaches are crucial in the analysis of cancer as a genetic disease and in the identification of patterns of gene expression that might be used in diagnosis and therapy. However, array-based analyses of whole tumors still treat the tumor as a black box. The discovery of specific genes that correlate with metastatic potential cannot be related to mechanism unless the metastatic step at the cellular level in which the gene is involved is identified. Ideally, high-resolution methods for the analysis of metastasis at the cellular level, such as imaging of cells within tumors, when combined with array-based approaches, could be used to accurately evaluate the roles of specific gene products in the individual steps of metastasis. To this end, the development of laser capture microdissection has been an important advance (6). However, the identification of cells within the tumor relies on morphology within fixed tissue, making the identity of the collected cells and their behavior within the tumor before fixation uncertain. Therefore, we have developed high-resolution methods for imaging cells within tumors.

We have used a model of breast cancer that allows the direct examination of the behavior of individual carcinoma cells in live nonmetastatic and metastatic primary tumors *in situ* (7, 8). The nonmetastatic and metastatic tumor cell lines used to create the tumors by s.c. injection are the MTC and MTLn3 cell lines, respectively. These cell lines represent a well-characterized cell pair that were derived from the same original tumor and retain their relative metastatic phenotypes after prolonged culture (9, 10). These cell lines were engineered to constitutively express GFP[5] (7). Upon s.c. injection of these cells into the mammary fat pad of female Fischer 344 rats, primary tumors form that contain fluorescent carcinoma cells. Furthermore, GFP expression does not affect the growth, histology, and metastasis of the primary tumor (7, 11, 12). With this model, the behavioral phenotypes of cells within metastatic and nonmetastatic tumors have been described and differentiated (7, 9). In principle, this model can be extended to any type of tumor cell that grows as a primary tumor s.c. It was the first model that allowed direct observations of invasive and metastatic cell behaviors in intact orthotopically grown primary tumors while in a live animal without the need for a viewing window and has made the primary tumor available for direct analysis at the single-cell level.

Recently, multiphoton microscopy, a powerful tool that combines laser scanning confocal microscopy with multiphoton excitation of fluorescence to create high-resolution, three-dimensional images of microscopic samples, has been introduced. This technique is particularly valuable in the study of cell behavior *in vivo* because it can be used to probe delicate living tissues at great depths and cellular resolution without damaging the sample (13, 14). In this study, we have combined our GFP-carcinoma cell models with multiphoton microscopy to image differences in cell behavior within the primary tumor. In addition, we have correlated differences in cell behavior with array-based approaches to directly associate cell behavior with gene expression and evaluate the roles of specific gene products in the individual steps of metastasis. This is the first time that these tech-

Received 5/16/02; accepted 9/11/02.

The costs of publication of this article were defrayed in part by the payment of page charges. This article must therefore be hereby marked *advertisement* in accordance with 18 U.S.C. Section 1734 solely to indicate this fact.

[1] Supported by United States Department of Defense Grant BC980718, NIH Grant CA 89829, grants from the National Institute of General Medical Sciences, and United States Department of Energy Grant DE-FG02-00ER63056. Real-time PCR was supported by Grant 1U24DK58768-01A1.

[2] Supplementary data for this article are available at Cancer Research Online (http://cancerres.aacrjournals.org).

[3] These authors contributed equally to this work.

[4] To whom requests for reprints should be addressed, at Department of Anatomy and Structural Biology, Albert Einstein College of Medicine, 1300 Morris Park Avenue, Bronx, NY 10461. E-mail: condeeli@aecom.yu.edu.

[5] The abbreviations used are: GFP, green fluorescent protein; ECM, extracellular matrix; QRT-PCR, quantitative real-time PCR; AECOM, Albert Einstein College of Medicine; NSI, net signal intensity; EGF, epidermal growth factor; EGFR, EGF receptor; FGF, fibroblast growth factor; IGF, insulin-like growth factor; PAK, p21/Cdc42/Rac1-activated kinase.

niques have been combined in this way. It is a novel approach to gene discovery in invasion and has made the primary tumor available for direct analysis at the single-cell level.

MATERIALS AND METHODS

Cell Culture and Tumor Growth. Rat mammary adenocarcinoma MTLn3 and MTC cell lines transfected with GFP were used in this study. Their metastatic potentials (high metastatic potential for MTLn3 cell line; low metastatic potential for the MTC cell line) have been described previously (9–11). Cells were maintained in α-modified MEM (Life Technologies, Inc.) containing 5% fetal bovine serum and antibiotics (penicillin and streptomycin). MTLn3 and MTC cells were injected into female Fischer 344 rats (1×10^6 cells/rat) as described previously, and tumors were allowed to grow for 2.5 weeks.

Anesthesia and Surgery of Tumor-bearing Animals. Tumor imaging was performed as described below. Briefly, 1×10^6 cells were injected under the second nipple anterior from the tail of a Fischer 344 rat and allowed to grow for 2.5 weeks. After 2.5 weeks, rats were placed under anesthesia with 5% isoflurane and maintained for the course of the imaging session at 2.5% to 0.5% isoflurane to control constant breathing. Minimal surgery was performed to expose the tumor by removing a small skin flap with as little damage to surrounding blood vessels as possible. The animal was placed on an inverted microscope and imaged at 960 nm for GFP fluorescence. For visualizing vasculature, 200 μl of rhodamine-dextran (2 M Dalton; Sigma Chemical Co.) at 20 mg/ml in Dulbecco's PBS were injected into the tail vein of the rat after anesthesia but before surgery.

Multiphoton Microscopy. A 10 W Millennium Xs laser (Spectra Physics) was used to run a Radiance 2000 multiphoton system (Bio-Rad, Hercules, CA) that gives an output of 850 mW at 960 nm. For GFP fluorescence, 960 nm is the optimal imaging wavelength. Time-lapsed images of GFP-labeled MTLn3- and MTC-generated tumors were taken at 60-s intervals for 30 min. The images were collected using Bio-Rad's Lasersharp 2000 software at 50 lines/s and a Kalman of 4. Images were processed using NIH Image 1.61/ppc and Adobe Photoshop. Pixel intensity of fluorescence and second harmonic-generated photons was quantified by subtracting the background from the total pixel intensity of the region of interest.

Measurement of Cell Behavior. Cell motility and adhesion were visualized by time-lapse multiphoton microscopy by taking an image at 1-min intervals for at least 30 min. Each Kalman averaged image required 10 s for collection giving good spatial resolution for cells moving 10 μm/min and less. Motion analysis was carried out using 2D DIAS image analysis software (15).

Microarray Procedures. Total RNA was isolated from MTLn3 and MTC cell or tumor using Trizol reagent (Life Technologies, Inc.). The RNA quality was verified by electrophoresis on a formaldehyde-1.2% agarose gel.

Microarray analysis was performed by using cDNA microarrays made at AECOM (16). About 9,700 mouse genes (Incyte Genomics) were precisely spotted onto a single glass slide. Detailed descriptions of microarray hardware and procedures are available online.[6] The use of these mouse arrays with rat RNA has been validated and shown to have more than 90% correlation between these two species.[7] This result was further validated by real-time PCR as described in this study (Fig. 7).

Microarray analysis was performed in three independent repeats. For each hybridization, cDNA targets were prepared from the RNA samples obtained from MTLn3 (Cy5-labeled) and the MTC (Cy3-labeled) cells or tumor. Labeling and hybridization were performed as follows: first-strand cDNA probes were generated by incorporation of either Cy3-dUTP or Cy5-dUTP (Amersham Pharmacia) during reverse transcription of 100 μg of total RNA. The resulting cDNA probes were purified and concentrated, denatured at 94°C, and hybridized to an arrayed slide overnight at 50°C. Slides were then washed in 1× SSC/0.1% SDS for 10 min and then washed in 0.2× SSC/0.1% SDS for 20 min. Slides were then rinsed and dried, and then they were ready for scanning. Data from the hybridization reactions were collected using a two-color laser scanning confocal microscope that was custom designed and built at AECOM specifically for the maximum sensitivity necessary to measure low abundance mRNAs. GenePix Pro 3.0 (Axon Instruments, Inc.) was used to generate raw data files containing measurements of signal and background fluorescence emissions of Cy3 and Cy5, respectively, for each element.

Quality Control, Data Analysis, and Statistics. Primary data were flagged using default parameters set in GenePix Pro 3.0 program. Normalization and data processing were performed as described previously (17, 18). Briefly, NSI of each spot in both channels (Cy5 as channel 1 and Cy3 as channel 2) was determined by subtracting the local background from signal intensity values and then subjected to log transformation. The overall intensity for each channel (I_{ch1} and I_{ch2}) was calculated by taking power of the average of the log of the NSI for all genes. The ratio of the overall intensity in channel 1 over that in channel 2 is calculated as $r = I_{ch1}/I_{ch2}$. The intensities for both channels were therefore balanced by multiplying the NSI of each spot in channel 2 by factor R. Under our experimental conditions, ratios of 1.6 and larger (up-regulated) or 0.6 and smaller (down-regulated) were chosen as significantly different gene expression levels between two samples hybridized to the same array spot (18). Genes showing consistent differential expression across replica arrays were extracted for further analysis. These genes were grouped on the basis of their function in cancer invasion and metastasis by searching PubMed, SwissProt database,[8] and Online Mendelian Inheritance in Man databases. Functional categories were correlated with cell behavior observed in the primary tumor and in culture.

QRT-PCR. To verify the data obtained from microarrays, QRT-PCR analysis of selected overexpressed and underexpressed genes (*ECM1, TIMP2, EGFR, Keratin 19, BMP1,* and *ZBP-1*) was performed by using the iCycler Apparatus (Bio-Rad) with sequence-specific primer pairs for all genes tested (see Supplemental Table 1 for primer sequences, amplicon size and melting temperature). Briefly, 5 μg of total RNA were converted into cDNA and used for the 40-cycle 3-step PCR in the iCycler apparatus. The SYBR Green PCR Core Reagents system (Perkin-Elmer Applied Biosystems) was used for real-time monitoring of amplification. Amplicon size and reaction specificity were confirmed by agarose gel electrophoresis. Each PCR reaction was repeated three times, and the median threshold cycle (C_T) values were used for analysis. Results were evaluated with iCycler IQ Real Time Detection System software (Bio-Rad).

Western Blots. MTLn3 and MTC cells were washed with ice-cold PBS before direct extraction in radioimmunoprecipitation assay buffer. Lysates were clarified by centrifugation, and protein concentrations were measured by bicinchoninic acid protein assay (Bio-Rad). Equal amounts of proteins were resolved by SDS-PAGE and transferred to nitrocellulose membrane. The membrane was blocked in 5% nonfat dried milk in Tris-buffered saline plus 1% Tween 20 and incubated with primary antibodies to ZBP-1 (Ref. 19; p62, a rabbit polyclonal antibody generated against full-length chicken ZBP-1), EF1-α (20), or Arp2/3 (Ref. 21; p34, a rabbit polyclonal antibody against Arp2/3 M_r 34,000 subunit) for 1 h, followed by incubation with appropriate conjugated secondary antibody for 1 h at room temperature. Immunoreactive bands were detected by chemiluminescence (New England Nuclear, Boston, MA), according to the manufacturer's instructions.

Differential Distribution of ZBP-1 in MTLn3 and MTC. The cells were propagated in serum and fixed and stained with anti-p62 antibody that detects ZBP-1. The tumors were grown in rats for 3 weeks after cell injection, and then they were surgically removed, sliced into approximately 1-mm slices, covered in OCT compound (Electron Microscopy Sciences), and frozen in isopentane on dry ice and ethanol. Then the tissue was cryosectioned into slices of 7–10 μm. Sections were fixed in 4% formaldehyde and stained with either anti-ZBP or anti-Arp 2/3 antibodies.

RESULTS

We have examined the motility of nonmetastatic and metastatic tumor cells in live primary tumors *in vivo*. Initial imaging was done using a conventional laser scanning pinhole confocal microscope (7, 8). Although confocal imaging can be effective in virtually eliminating out-of-focus light from thick objects, which is necessary for intravital imaging, this technique does nothing to alleviate another major problem of intravital imaging, phototoxicity. The technique of

[6] http://www.aecom.yu.edu/home/molgen/facilities.html.

[7] M. Dabeva, personal communication.

[8] http://ca.expasy.org/sprot/.

multiphoton excitation provides an elegant solution to the problem of phototoxicity by preventing unwanted out-of-focus excitation. Excitation is confined only to the optical section being observed (13, 22). The sample is illuminated with light of a wavelength that is approximately twice (or three times) the wavelength of the absorption peak of the fluorophore in use. In the case of GFP, which has an absorption peak at approximately 480 nm, 960 nm light can be used for excitation. Essentially no excitation of the fluorophore will occur at the 960 nm wavelength out of the plane of focus because this wavelength is thus far removed from GFP's peak excitation wavelength. In addition, no bleaching will occur, nor will phototoxic products be generated in the bulk of the sample. A high peak power laser source is used in pulses that are shorter than a picosecond so that the mean power levels are moderate and do not damage the specimen. With this source, the photon density only at the point of focus will be sufficiently high for significant numbers of two photon events to occur to generate fluorescence. Out-of-focus interference is eliminated simply because it is never generated.

Comparison of Conventional Confocal and Multiphoton Microscopes in Intravital Imaging of Intact Mammary Tumors

Comparison of the laser scanning confocal microscope with the multiphoton microscope for imaging of primary mammary tumors was done in live anesthetized rats with 2.5-week-old tumors (Fig. 1). In both imaging techniques, we found that GFP in the tumor cells is an excellent cytoplasmic volume marker that allows the entire cell outline to be defined *in vivo* in the living intact tissue (7, 8).

Fig. 1*A* shows two series of optical sections obtained by stepping at 12-μm intervals through a primary tumor in a live animal. The *left panels* were obtained with the conventional confocal microscope, and the *right panels* were obtained with the multiphoton microscope using an infrared laser and an external detector to avoid the confocal pinhole. Comparison of these two z-series demonstrates the superiority of the multiphoton microscope in penetrating deep within the live tissue to generate high-resolution confocal images. The greater depth of imaging of the multiphoton microscope compared with the confocal microscope is impressive when one considers that the z-series obtained with the multiphoton was started 36 μm inside of the primary tumor and not at the surface, the point at which the signal from the confocal microscope has fallen away. Hence, whereas the deepest useful image possible with the conventional confocal microscopy was <40 μm, we have obtained useful images from depths of up to 300 μm with the multiphoton microscope (Fig. 2*E*). In addition, signal:noise ratio does not fall off significantly throughout the z-series obtained with the multiphoton microscope.

Fig. 1*B* shows two series of optical sections identical to those in Fig. 1*A* but repeated to demonstrate the relative amount of bleaching occurring upon reexposure of the same optical planes to laser light. The confocal z-series (*left panels*) is significantly bleached by repeated imaging, whereas the multiphoton z-series (*right panels*) has usable signal: noise ratio at all depths. Therefore, the bleach rate is much less in the multiphoton microscope. In addition, these results demonstrate that with the imaging conditions used to document cell behavior in this study, bleaching does not affect the interpretation of time-lapse images.

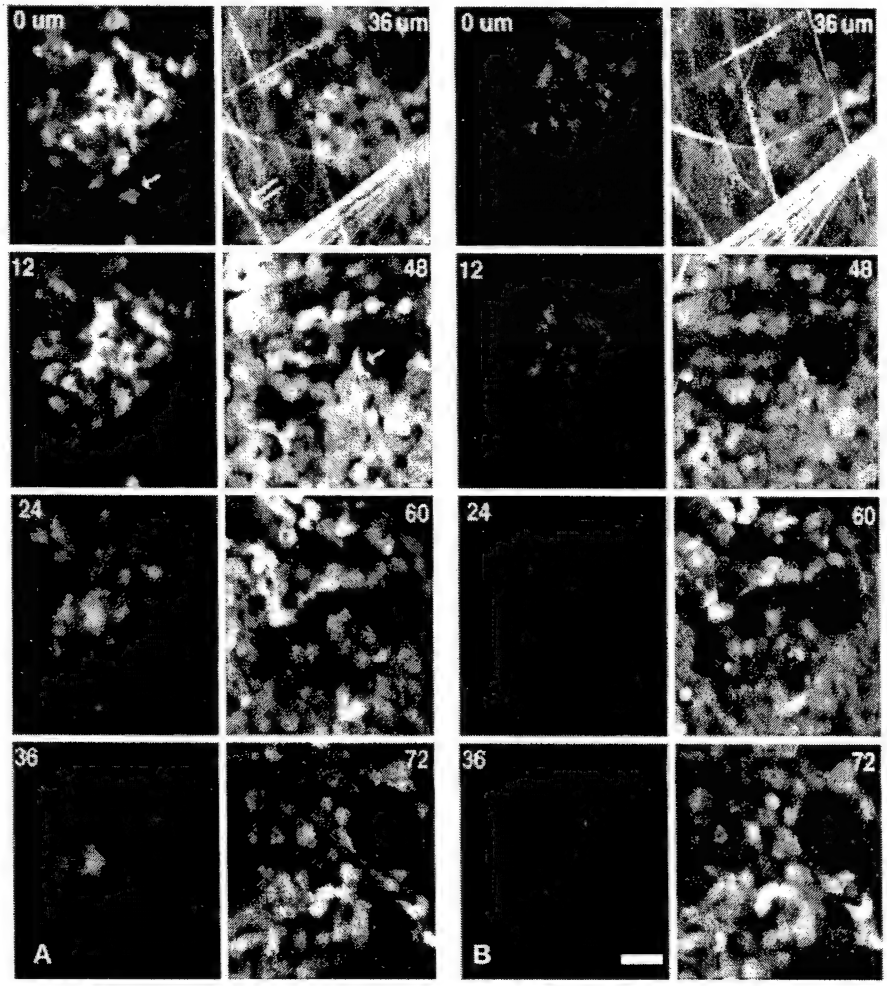

Fig. 1. Multiphoton microscopy is superior in imaging primary tumors more deeply and with less photodamage. *A*, initial z-series of images taken with the confocal (*left panels*) and multiphoton (*right panels*) microscope showing the greater depth of imaging possible with multiphoton excitation. The confocal microscope can only image to approximately 36 μm. The first panel of the multiphoton images (*top right panel*) begins at 36 μm and shows an image of better quality than that of the confocal image at 0 μm (*top left panel*). *Arrows* point to a single cell. *Double arrow* points to ECM seen only in multiphoton microscopy due to second harmonic generation. *B*, second z-series of the same focal planes illustrates dramatic improvement in GFP stability (*right panels*) in the multiphoton microscope compared with (*left panels*) the confocal microscope.

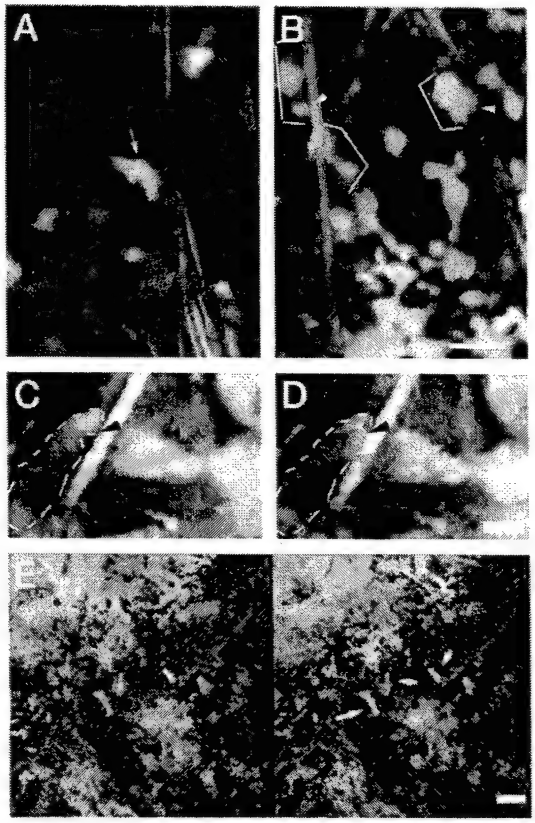

Fig. 2. Carcinoma cells in MTLn3 tumors adhere to ECM, extend pseudopods, and exhibit linear excursions toward blood vessels. Carcinoma cells in MTC (*A*) and MTLn3 (*B–E*) tumors were imaged by multiphoton microscopy. *A*, carcinoma cells in MTC tumors do not attach or orient on collagen-containing ECM fibers *in vivo*. A single fiber can be seen bending around the cell. The *arrow* points to collagen fiber bent over cell. *B*, carcinoma cells in MTLn3 tumors are observed to contact collagen-containing fibers. *Arrowheads* point to cell-matrix interactions. Elongated cells are highlighted by *brackets*. *Scale bar*, 25 μm. *C*, carcinoma cell is seen attached to matrix fiber (*black arrowhead* in *C*). The cell is delineated by the *white dotted line*. *D*, 4 min later, the carcinoma cell has spread along the fiber by approximately 8 μm. The *red arrowhead* shows the position of attachment after 4 min. The *black arrowhead* in *D* indicates the original attachment site in *C*. *Scale bar*, 10 μm. *E*, in a stereo pair image, GFP-labeled carcinoma cells are observed entering a rhodamine-dextran-filled blood vessel. The cells (*green*) are seen on the surface of the blood vessel (*red*) with pseudopodia (*yellow*) elongating into the vessel. *Arrows* point to cells entering blood vessel. The image is a 120-μm stack of 30 optical planes, each taken with a multiphoton microscope and then rendered as a stereo pair. The initial depth of the image is >100 μm. The blood space was labeled by injecting 2 M Dalton rhodamine-dextran i.v. into the blood space. *Scale bar*, 25 μm.

Differences in Carcinoma Cell Behavior in Metastatic and Nonmetastatic Primary Tumors

Intravital imaging of the behavior of cells in the MTC (nonmetastatic)- and MTLn3 (metastatic)-derived tumors demonstrates significant differences between the two. One of the advantages of multiphoton microscopy of intact tissue is the ability to image ECM-containing collagen by second harmonic generation (14, 23). As shown in Fig. 2, *A* and *B*, some carcinoma cells in MTLn3 tumors are closely associated with collagen fibers, whereas cells in MTC tumors do not associate. Rare interactions between carcinoma cells in MTC tumors and collagen fibers do not involve the movement of cells along the fiber, and the cells seem to push the fibers out of the way as they move (Fig. 2*A*). In metastatic MTLn3 tumors, the carcinoma cells move individually when in contact with collagen fibers (Fig. 2*B*, *arrowheads*). High-resolution time-lapse images of carcinoma cell movement on a collagen fiber are shown in Fig. 2, *C* and *D*, and they demonstrate the cell-collagen fiber interactions and linear locomotion exhibited *in vivo* by carcinoma cells in MTLn3 tumors. This result is consistent with the streaming like linear cell locomotion shown previously in MTLn3 tumors with conventional confocal microscopy (7). In these earlier studies, we were unable to see the underlying fibers that caused the linearity of motion.

The average instantaneous velocity of carcinoma cells from four different metastatic MTLn3 primary tumors was measured as 3.4 μm/min. However, in all of the tumors examined, it was apparent that only a small fraction of carcinoma cells in the primary tumor are actively motile during any given imaging interval. For some of these cells, instantaneous velocity values were close to the persistence value, indicating a high degree of rectilinear motion reminiscent of chemotaxis (15). The velocities of ~3.4 μm/min shown by carcinoma cells in the MTLn3 primary tumor are higher than the velocities exhibited by these cells in culture during either random motility (0.45 ± 0.08 μm/min, $n = 8$) or highly persistent motility (0.82 ± 0.19 μm/min, $n = 8$) observed in a gradient of EGF, which is chemotactic for these metastatic adenocarcinoma cells (24).

Carcinoma cells in MTC tumors move at rates similar to those in MTLn3 tumors, but the character of the cell motility is quite different. In MTC tumors, the cells move over each other, and the direction of motility is not linear and does not appear to be guided by collagen fibers (Figs. 2*A* and 4). The long linear excursions of carcinoma cells along collagen fibers and in association with vessels (Fig. 2, *C–E*, and Fig. 3) seen in MTLn3 tumors are not observed in MTC tumors (Fig. 4). There is no motility in MTLn3 tumors in areas where there are no vessels or collagen fibers. This is a major difference between the metastatic MTLn3 and nonmetastatic MTC tumors.

Differences in Intravasation by Carcinoma Cells in Metastatic and Nonmetastatic Primary Tumors

A strong correlation exists between the density of live carcinoma cells in the blood and the number of both single cells and metastases in the lungs, establishing intravasation as a key step for metastasis (8). Chemotaxis of carcinoma cells within the primary tumor toward growth factors such as EGF that are associated with blood vessels and

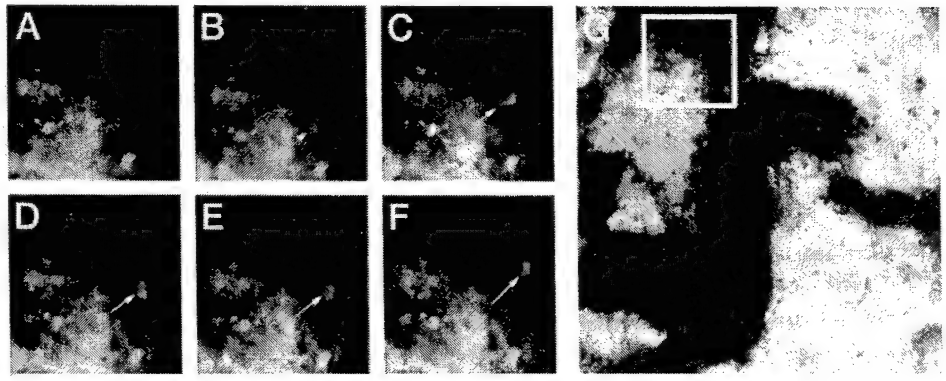

Fig. 3. Time-lapse imaging of intravasation of carcinoma cells in MTLn3 tumors. *A–F*, using multiphoton imaging, a single carcinoma cell (*green*) is seen crawling along a blood vessel. The *arrows* show the direction and the distance the cell moved along the vessel. Images were taken 5 min apart. *Scale bar*, 25 μm. *G*, the full field is shown to orient the area in which the cell in *A–F* is shown. Blood vessels are seen as *black areas* through carcinoma cell cords (*green*). The *white box* delineates the area seen in *A–F*.

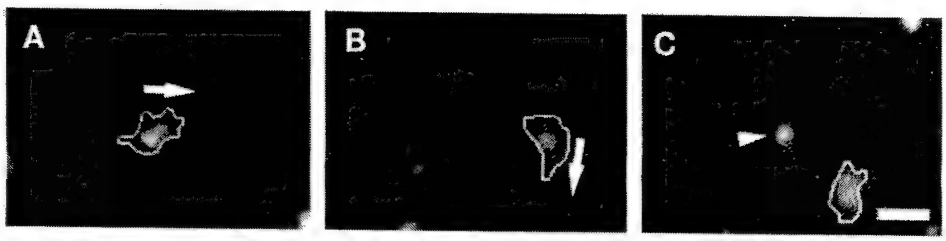

Fig. 4. Carcinoma cells in MTC tumors exhibit random motility with no relationship to either ECM or vessels. *A–C, white line* outlines the perimeter of a moving cell, whereas *arrows* show the direction of movement. Another cell is seen moving into the plane of focus C (*arrowhead*). Each frame is 4 min apart. *Scale bar,* 25 μm.

differences in the ability of carcinoma cells to resist lysis upon intravasation were proposed to be responsible for this correlation (8). Supporting chemotaxis are the observations of dramatic polarity of carcinoma cells toward blood vessels only in metastatic MTLn3 tumors and the high rates of chemotaxis of carcinoma cells measured within the primary tumor toward microneedles containing EGF and Matrigel (8, 25). To investigate the interaction of carcinoma cells with blood vessels in metastatic MTLn3 primary tumors in more detail and to determine if carcinoma cells have the intrinsic ability to locomote toward blood vessels and intravasate without fragmentation, we used GFP expression by carcinoma cells and multiphoton microscopy to time-lapse image the behavior of single carcinoma cells near blood vessels in the MTLn3 primary tumor. As shown in Fig. 2*E,* carcinoma cells are elongated and polarized toward blood vessels, suggesting that there is a vessel-mediated attraction for the cells. The depth of imaging possible with the multiphoton microscope illustrates, in the three-dimensional projection in Fig. 2*E,* that many of the carcinoma cells cross the vessel wall as intact single cells. That this is an active process requiring each cell to cross an intact vessel wall is shown by the failure of i.v. injected low molecular weight fluorescent dextran to escape from the vessels during intravasation (Fig. 2*E*). Furthermore, time-lapse imaging of cells in contact with blood vessels demonstrates the ability of carcinoma cells to actively crawl into the blood vessel using amoeboid locomotion (Fig. 3). Finally, fragmentation of carcinoma cells, as observed in MTC tumors during intravasation (8), was not observed in metastatic MTLn3 tumors. All of these results correlate directly with the large number of GFP-expressing carcinoma cells observed in the circulation of the MTLn3 primary tumors (Fig. 5) and their absence from the vessels of MTC tumors (8).

Differences in ECM between Metastatic and Nonmetastatic Primary Tumors

To estimate the amount of ECM present in the primary tumor, we used second harmonic generation to image collagen fibers in the primary tumor *in vivo* (14, 23). As shown in Fig. 6, the amount, integrity, and size of the collagen fibers in the second harmonic image were reduced in MTLn3 compared with MTC tumors. As shown in Fig. 6*C,* metastatic MTln3-derived tumors have 2.4 times less collagen than MTC tumors. This is consistent with the general observations that the MTC tumors are more fibrous and less necrotic and that the clusters of carcinoma cells in MTC tumors are far apart due to intervening large collagen arrays (Figs. 2 and 6). However, as shown in Fig. 1, large amounts of collagen are observed near the outside edge of MTLn3-generated tumors, where the cells are seen adhering to and elongated on the collagen fibers.

Summary of Behavioral Differences

Based on the multiphoton microscope observations reported here and on previous studies with the same tumor models (8, 25), there are five major differences in cell behavior between the MTLn3- and MTC-derived primary breast tumors: (*a*) in MTLn3 tumors, some carcinoma cells are associated with collagen fibers, whereas in MTC tumors, this is not observed; (*b*) linear cell motility is seen along collagen fibers in MTLn3 tumors; (*c*) there is increased carcinoma cell polarity and locomotion toward blood vessels in metastatic MTLn3 tumors, whereas carcinoma cells in MTC tumors appear oriented toward each other, but not toward vessels; (*d*) carcinoma cells in MTLn3 tumors remain intact during intravasation, whereas carcinoma

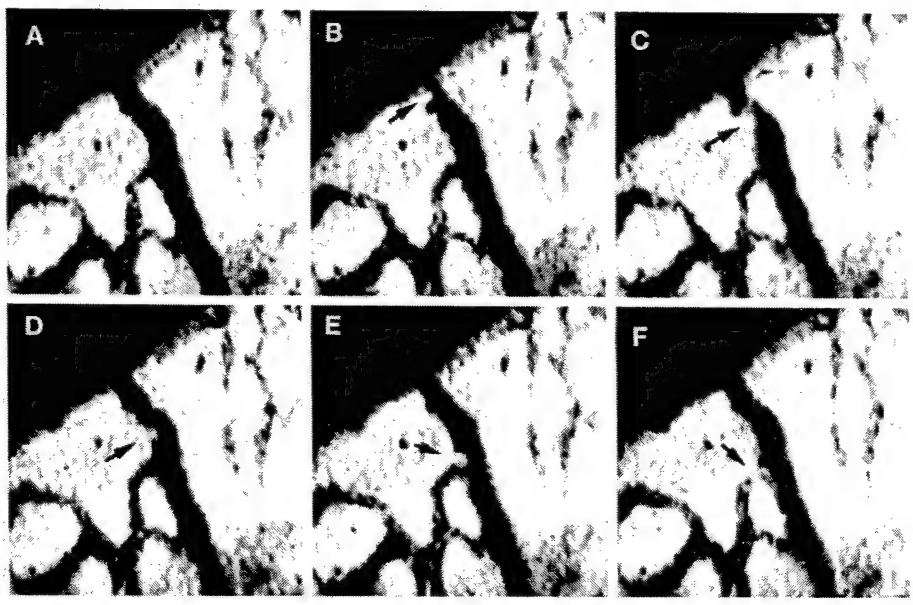

Fig. 5. Intact GFP-expressing carcinoma cells are routinely observed in the circulation of MTLn3 primary tumors. A GFP-labeled carcinoma cell can be seen rolling down the side of a vessel. The vessels are imaged by contrasting the vessels against the fluorescent tumor using a SIT camera and capturing frames at 30 frames/s. The cell moves through the vessel at 3.3 μm/s. Carcinoma cells are seen in blood vessels 6-fold more often in MTLn3 tumors than in nonmetastatic MTC tumors, appearing at a rate of 2.2 ± 0.72 cells/min in MTLn3 as compared with 0.34 ± 0.13 cells/min for MTC tumors. *Scale bar,* 25 μm.

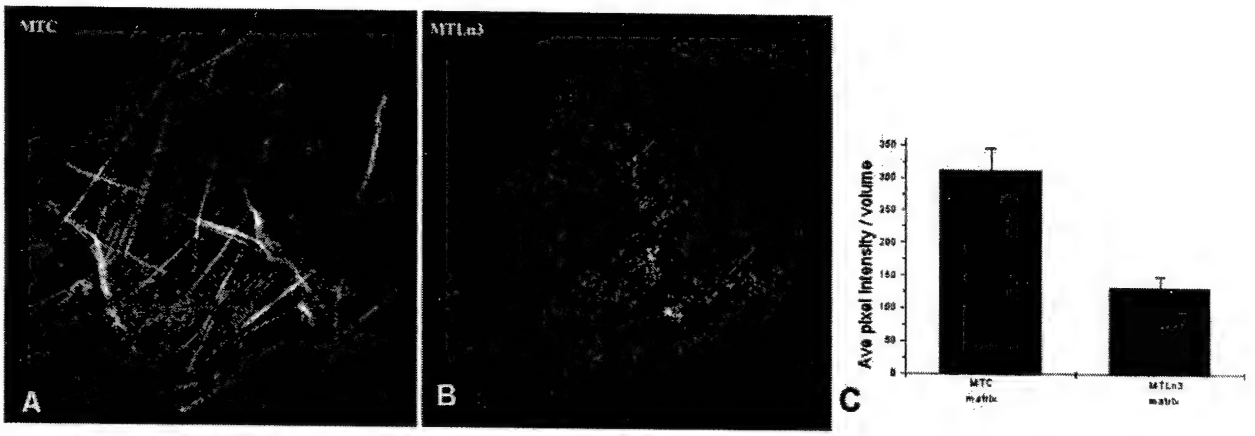

Fig. 6. MTC tumors have more collagen-containing ECM than MTLn3 tumors. By imaging the second harmonic signal of ECM using multiphoton microscopy, the difference in collagen content between the two tumor types was determined. *A*, MTC tumors at 35 μm depth into the tumor can be seen to have more matrix than (*B*) MTLn3 tumor at the same depth of focus. The images were collected through a blue/green dichroic with a wavelength cutoff below 500 nm, so only the second harmonic signal was collected. The tumors used to generate these images did not contain GFP to avoid stray fluorescence. *C*, by calculating the pixel intensity for the captured volume of a z-series of each tumor, MTC tumors are seen to have on average of 2.4 times more matrix than MTLn3-generated tumors. $n = 4$. The laser power and photomultiplier tube gain were constant for all measurements.

cells in MTC tumors fragment; and (*e*) collagen fiber density is higher in MTC tumors. These behavioral differences predict seven categories of molecular differences between metastatic and nonmetastatic tumors as follows: (*a*) ECM composition; (*b*) adhesion molecules; (*c*) cytoskeleton involved in motility; (*d*) mechanical stability and survival; (*e*) cell polarity; (*f*) chemotaxis toward vessels; and (*g*) proteolysis of collagen.

Identification of Differentially Expressed Genes in Metastatic and Nonmetastatic Primary Tumors and Their Progenitor Tumor Cells

To obtain a profile of differential gene expression that is associated with the behavioral differences observed between MTLn3- and MTC cell-derived primary tumors, whole primary tumors were isolated from host animals and subjected to cDNA microarray analysis on 9700 gene arrays. We also studied the cultured cells from which the primary tumors were derived because they are a more homogeneous cell population than whole tumors (24). Comparative differential gene expression analysis of metastatic and nonmetastatic tumors and their progenitor cells in culture revealed only 161 genes with differential expression patterns in both tumors and their progenitor cells in culture. Supplemental Table 2 shows the complete list of differentially expressed genes. Of these, 119 genes are more highly expressed (at least 1.6×) in MTC compared with MTLn3 tumors, and 42 genes are more highly expressed (at least 1.6×) in MTLn3 compared with MTC tumors. Among the genes with known functions, at least 70 of them (shown in bold in Supplemental Table 2) are known to be involved in cancer invasion and metastasis. In addition, 61 expressed sequence tags of unknown function also showed different patterns of expression. To relate cell behavior to gene expression, in this study we therefore focused on the genes of known function and related them to each of the behavioral phenotypes seen *in vivo*.

Validation of Array Data by QRT-PCR

We verified the array results using real-time PCR for selected genes. As shown in Fig. 7, in general, most genes showed the same pattern of expression with both array and real-time PCR. However, studies have shown that fluorescent dye-based microarrays can be less sensitive than the PCR-based differential display method in detection of low abundance mRNA species (26). One of these mRNAs, ZBP-1, which regulates cell polarity by targeting mRNA to the leading edge, has been shown to be overexpressed in most tumors and can be used as a novel human tumor marker (27–29). Our microarrays detected larger differences in culture than in the primary tumors in ZBP-1 expression, whereas real-time PCR reproducibly showed a large increase in expression in both cultured MTC cells and whole MTC tumors.

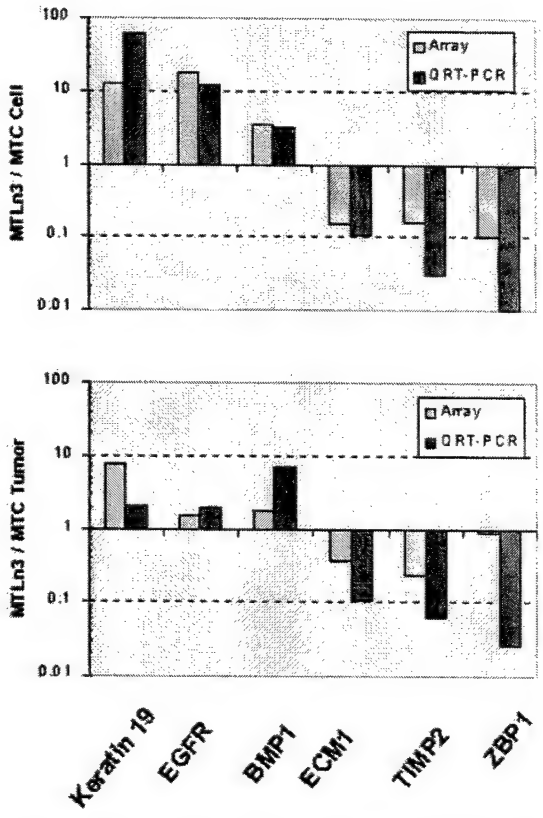

Fig. 7. Validation of microarray results for selected genes by QRT-PCR. Comparison of expression analyses in cells in culture (*top panel*) and whole tumors (*bottom panel*) gives similar results for cDNA microarrays and QRT-PCR, except for low abundance mRNAs such as ZBP-1.

Correlation of Cell Behavior with Gene Expression Patterns

Imaging of cell behavior within the tumor provided a way to interpret the cDNA microarray analyses. In this approach, genes with different expression patterns and known cellular functions were divided into seven categories of genes predicted from the behavior of carcinoma cells *in vivo* (Table 1).

ECM Composition. A major behavioral difference between MTC and MTLn3 tumors is the abundance of collagen fibers in MTC tumors. Consistent with this is the overexpression of several collagen genes involved in ECM assembly (*Col3a1, Col5a2,* and *Col6a3*) in MTC tumors and cells in culture (Table 1).

Two laminin genes, *Lama5* and *Lamc2*, are found to be differentially expressed in these two tumor types. *Lama5*, encoding laminin α-5, is more highly expressed in MTC cells and tumors. *Lamc2* gene, encoding laminin-5 γ2 chain, is found to be more highly expressed in MTLn3 tumors and cells in culture (Table 1). The laminins are components of basement membranes that are believed to act as a mechanical barrier against carcinoma cell invasion (4). Laminin-5 is also reported to stimulate cell migration after proteolysis. Two other genes highly expressed in MTC tumors and cells are *Ecm1* encoding ECM protein 1 and *Comp* encoding cartilage oligomeric matrix protein (Table 1).

Adhesion Molecules. In the category of adhesion molecules, both E-cadherin and P-cadherin show much higher expression in MTLn3 cells and tumors (Table 1). MTLn3 tumors and cells also express more of tight junction protein 2, a protein that may play a critical role in cell-cell adhesion (30). Two other major adhesion molecules, CD151 and Adam19, were found to be highly expressed in MTC tumors and

Table 1 *List of genes that are differentially expressed and correlated with cell behavior in MTLn3 and MTC tumors*

Gene functions are based on NCBI PubMed, SwissProt data base (http://ca.expasy.org/sprot/) and Online Mendelian Inheritance in Man (*http://www.ncbi.nlm.nih.gov/omim/*). NC, no change detected by array. Numbers in parentheses indicate the changes detected by QRT-PCR.

Gene names organized by gene function	GenBank accession no.	Protein	Mean MTLn3:MTC (culture)	Mean MTLn3:MTC (tumor)
ECM composition				
Col3a1	W89883	Collagen, type III, α 1	0.01	0.15
Col5a2	AA034564	Collagen, type V, α 2	0.05	0.19
Col6a3	W16221	Collagen, type VI, α 3	0.22	0.11
Lamc2	W49392	Laminin, γ 2	4.23	1.74
	W09048	Laminin, γ 2	3.18	1.96
Lama5	AA049251	Laminin, α 5	0.52	0.53
Ecm1	AA474897	ECM protein 1	0.09	0.37
Comp	AA064293	Cartilage oligomeric matrix protein	0.31	0.60
Adhesion molecules				
Cdh3	W12889	Cadherin 3, P-cadherin	9.19	3.00
Cdh1	AA276110	Cadherin 1, E-cadherin	9.82	3.31
Tjp2	W91219	Tight junction protein 2	2.96	2.16
Cd151	AA050218	CD151 antigen	0.16	0.29
Adam19	AA138786	A disintegrin and metalloproteinase domain 19	0.13	0.41
Cytoskeleton involved in motility				
EST	W47753	AR16_Human ARP2/3 complex M_r 16,000 subunit	6.31	5.45
Cappa1	AA414612	Capping protein 1	NC	2.65
Cttn	W96939	Cortactin	0.23	0.58
Pfn2	AA139628	Profilin 2	0.22	0.35
Rock2	AA098168	Rho-associated coiled-coil forming kinase 2	NC	2.13
Mechanical stability and survival				
Krt1-19	AA028346	Cytokeratin 19	12.30	7.97
Krt1-13	AA080232	Cytokeratin 13	NC	2.79
Krt2-1	W63927	Keratin complex 2, basic, gene 1	0.24	0.43
Rab25	AA538228	Member Ras oncogene family	7.99	6.38
Rab19	AA118762	Member Ras oncogene family	2.26	1.66
Bcl2l10	AA426964	BCL2-like10	NC	3.07
Met	AA212170	Met proto-oncogene	2.55	1.96
EST	AA471761	Cellular apoptosis susceptibility protein	0.62	0.64
Pdcd	AA465936	Programmed cell death 4	0.30	NC
Cell polarity				
Zbp1(crdbp)	AA073514	Zip code-binding protein 1	0.08	NC (0.027)
Stau1	AA270608	Staufen	0.48	NC
Eef1a1	AA259551	EF1-α	NC	2.69
Chemotaxis toward vessels				
Egfr	AA237224	EGFR	20.12	NC (2.0)
EST	AA059642	EGFR-pathway-substrate 8, EPS8	NC	2.77
Cav	AA138693	Caveolin, caveolae protein, M_r 22,000	0.04	0.17
Pak1	AA061378	PAK1 serine/threonine kinases	0.28	0.53
Mapk7	AA395937	Mitogen-activated protein kinase 7	0.57	0.39
Fgfr1	AA272097	FGF receptor 1	0.32	0.35
Igfbp5	AA241784	IGF-binding protein 5	0.15	0.14
Lef1	AA119479	Lymphoid enhancer-binding factor 1	0.11	0.26
Gpcr26	W97046	G-protein-coupled receptor 26	0.14	0.20
Gtr2	W70912	Small GTPase	0.46	0.45
Tbk1	AA475369	TANK-binding kinase TBK1	0.45	0.52
EST	AA049480	Bone morphogenetic protein 3 precursor	0.06	0.44
	W13196		0.04	0.35
Spp1	AA108928	Secreted phosphoprotein 1, also as osteopontin (OPN)	0.03	0.07
9-sep	W33661	Septin 9	0.18	0.42
Proteolysis of collagen				
Bmp1	W82677	Bone morphogenetic protein 1	3.49	1.72
Spi4	AA218279	Serine protease-inhibitor 4	0.03	0.11
Timp2	AA444490	Tissue inhibitor of metalloproteinase 2	0.16	0.19
Cst3	W78651	Cystatin 3	0.08	0.22
Mmp2	W80177	Matrix metalloproteinase 2	0.03	0.15

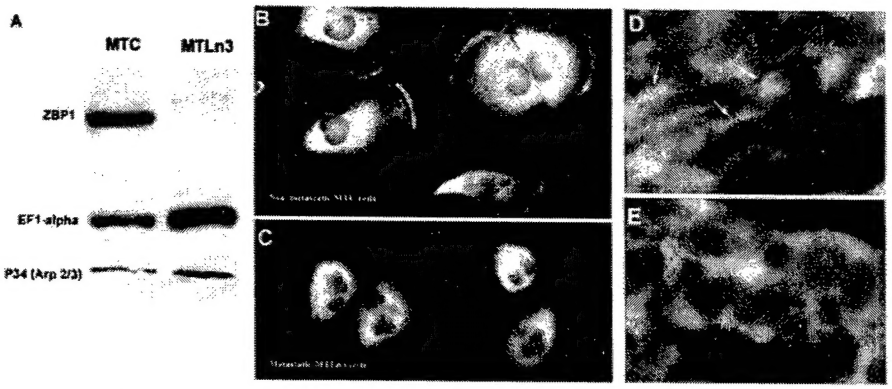

Fig. 8. ZBP-1, EF1-α, and Arp2/3 are differentially expressed at the protein level in MTLn3 and MTC cells. ZBP-1 is localized to the polarized leading edge of carcinoma cells in MTC tumors. Whole cell extracts from MTLn3 and MTC cells were resolved by SDS-PAGE and subjected to immunoblotting with polyclonal antibodies against either ZBP-1, EF1-α, or Arp2/3 p34 subunit to detect their expression at the protein level. ZBP-1 shows higher expression in MTC cells (MTC:MTLn3 ratio > 13), whereas EF1-α (MTLn3:MTC ratio = ~1.5) and Arp2/3 p34 (MTLn3:MTC ratio = ~2) show more expression in MTLn3 cells. MTC cells (*B*) and MTLn3 cells (*C*) were fixed and stained with anti-p62 antibody that detects ZBP-1. ZBP-1 is localized to the leading edge of MTC cells, whereas MTLn3 cells show a diffuse distribution. MTC tumors (*D*) and MTLn3 tumors (*E*) were grown in rats for 3 weeks and then surgically removed, cryosectioned, and stained with anti-p62 antibody that detects ZBP-1. Note the polarized distribution of ZBP-1 to one pole of each cell only in carcinoma cells of MTC tumors (*arrows*).

cells (Table 1). Transmembrane 4 superfamily protein CD151 associates with β_1 and $\alpha_{IIb}\beta_3$ integrins in hemopoietic cell lines and modulates cell-cell adhesion (31). Adam19/adamalysin-19 (a disintegrin and metalloproteinase) is involved in proteolysis, adhesion, fusion, and intracellular signaling (32).

Cytoskeleton Involved in Motility. Microarray analysis shows that the M_r 16,000 subunit of the Arp2/3 complex is greatly overexpressed in MTLn3 cells and tumors (Table 1). Because the p16 subunit is the only Arp2/3 component spotted on the array, we tested the expression level of subunit p34, a marker for the Arp2/3 complex (33), at the protein level using Western blotting. These results indicate that MTLn3 cells express at least 2-fold more p34 at the protein level (Fig. 8*A*). Capping protein is more highly expressed in MTLn3 tumors, but not cells (Table 1). Capping protein caps the barbed ends of actin filaments to regulate actin dynamics (34).

Another gene highly expressed in MTLn3 tumors is *ROCK2* (Table 1). ROCK2, an isozyme of ROCK1, is a direct downstream target of Rho (35).

Cortactin is involved in stimulating the binding of activated Arp2/3 complex to the sides of actin filaments to decrease debranching (36). Unlike the Arp2/3 complex, cortactin was more highly expressed in MTC cells and tumors (Table 1).

Profilin was also more highly expressed in MTC cells and tumors (Table 1). Profilin increases the on-rate of actin monomers at the barbed end sufficiently to lower the critical concentration for actin polymerization (34).

Mechanical Stability and Survival. MTLn3 cells and tumors exhibit dramatic overexpression of keratins 19 and 13, whereas MTC cells and tumors express a higher level of keratin complex 2 (Table 1). In addition, the array data show that MTLn3 cells and tumors express more apoptosis suppressors such as Rab19, Rab25, BCL2l10, and Met (37). Also consistent with cell fragmentation in MTC tumors, MTC cells and tumors express more programmed cell death and cellular apoptosis susceptibility proteins such as Pdcd and Casp (cellular apoptosis susceptibility protein).

Cell Polarity. ZBP-1 and staufen expression in MTLn3 cells was much lower compared with MTC cells in culture (Table 1). To detect differences in expression of this low abundance message in tumors, QRT-PCR was used for ZBP-1 as described above and shown in Fig. 8. A very large overexpression of ZBP-1 was demonstrated in both MTC cells and tumors compared with MTLn3 samples. ZBP-1 is a RNA-binding protein that binds to the mRNA zip code and functions to localize β-actin mRNA (19). Mammalian Staufen is a double-stranded RNA-binding protein potentially involved in mRNA transport and localization (38).

To confirm the increased expression of ZBP-1 at the protein level in MTC cells and tumors, immunohistochemistry was performed using anti-ZBP-1 antibody in both cultured cells and tumors. The pixel intensity showed that in cultured cells, MTC cells and carcinoma cells in MTC-generated tumors express more ZBP-1 compared with MTLn3 cells. Western blots also showed that MTC cells express 13-fold more ZBP-1 than MTLn3 cells (Fig. 8*A*). In addition, as shown in Fig. 8, *B–E,* ZBP-1 was found to be polarized in MTC cells in culture and in carcinoma cells within the primary tumor, whereas ZBP-1 was diffusely distributed in both MTLn3 samples.

A related protein, EF1α, was found to be more highly expressed in MTLn3 cells (Table 1), which is consistent with its overexpression at the protein level in MTLn3 cells (20). EF1α is an elongation factor that is involved in mRNA anchorage at the leading edge in polarized cells, and its overexpression in correlated with delocalization of mRNA (39).

Chemotaxis toward Vessels. Another major behavioral difference was chemotaxis to EGF of MTLn3 cells but not MTC cells as observed both in culture and in tumors (24, 25). Consistent with this, expression data showed significant differences in the expression of genes encoding chemotaxis and signal transduction molecules that are known to play roles in cancer invasion and metastasis (Table 1). The high level of EGFR in MTLn3 cells is consistent with previous studies (40). EGFR signaling involves small GTPases of the Rho family, and EGFR trafficking involves small GTPases of the Rab family. Lanzetti *et al.* (41) reported that the EPS8 (EGFR pathway substrate 8) protein coordinates EGFR signaling through Rac and trafficking through Rab5. We detected 3-fold more expression of EPS8 in MTLn3 tumors compared with MTCs.

Array analysis shows that caveolin is highly expressed in MTC cells and tumors (Table 1). Caveolin-1 is a principal component of caveolae membranes and may function as a tumor suppressor. Interestingly, MTLn3 cells fail to express detectable levels of endogenous caveolin-1. In a recent study (42), an inducible adenoviral gene delivery system was used to achieve tightly controlled expression of caveolin-1 in MTLn3 cells. Caveolin-1 expression in MTLn3 cells inhibits EGF-stimulated lamellipod extension and cell migration and blocks anchorage-independent cell growth. This result suggests that caveolin-1 expression in MTC cells causes a nonmotile phenotype.

PAK1, which is more highly expressed in MTC tumors and cells (Table 1), promotes the disassembly of stress fibers and focal adhesions. PAKs may regulate cytoskeletal dynamics by decreasing myosin light chain kinase activity and myosin light-chain phosphorylation (43).

Other signaling genes more highly expressed in MTC tumors and cells (Table 1) are genes encoding FGF (*FGF*), IGF-binding protein 5 (*IGFBP5*), mitogen-activated protein kinase 7, lymphoid enhancer factor 1 (*Lef1*), G protein-coupled receptor 26 (*Gpcr26*), glutamyl-tRNA reductase 2 (*Gtr2*), Tank binding kinase (*Tbk1*), and bone morphogenetic protein 3 (*Bmp3*). They are documented to be involved in different signaling pathways. *Spp1*, the gene encoding secreted phosphoprotein 1, a phosphorylated glycoprotein with diverse functions in cell adhesion and chemoattraction, is highly expressed in MTC tumors and cells (Table 1). Septin 9 is also highly expressed in MTC samples. It is implicated in a variety of cellular functions involving specialized regions of the cell cortex and changes in cell shape.

Proteolysis of Collagen. MTLn3 cells express much more BMP1 than MTC (Table 1). The *BMP1* locus encodes a procollagen C proteinase, a secreted metalloprotease requiring calcium (44, 45). A recent study (45) found that BMP1 cleaves the laminin-5 (LAMA3) chain at sites within the G4 subdomain and the IIIa domain and that BMP1 cleaves the LAMC2 chain within the second EGF-like repeat of domain III. Consistent with the observation of more intact collagen in MTC tumors is the finding that Spi4, Cst3, and TIMP2, all inhibitors of proteinases, are overexpressed in MTC cells and tumors compared with MTLn3 samples (Table 1). TIMP 2, a M_r 21,000 protein that is secreted by melanoma cells and binds to type IV collagenase proenzyme secreted by the same cells, has been shown to block tumor cell invasion both *in vitro* and *in vivo*, suggesting that it acts as metastasis suppressor gene. However, Mmp2 encoding matrix metalloproteinase-2 (MMP2 or type IV collagenase, M_r 72,000), is also highly expressed in MTC tumors and cells (Table 1).

DISCUSSION

The Interaction of Carcinoma Cells with ECM. Carcinoma cells in metastatic MTLn3 tumors are associated with and locomote on collagen-containing fibers, whereas this is not seen in MTC tumors. This suggests that either adhesion molecules mediating the attachment of carcinoma cells to collagen-containing ECM are different or the signals for cell adhesion and motility associated with collagen-containing fibers are different between MTC and MTLn3 tumors. The array analysis did not detect any large differences in integrin receptor expression, which is inconsistent with the first possibility.

A large increase in cadherin expression was found in MTLn3 tumors and cells. Cadherins are a family of calcium-dependent adhesion molecules involved in cell-cell aggregation and epithelial formation. Dysfunction of the cadherin pathway is involved in tumor invasiveness and disease progression for a variety of carcinomas (46). High levels of cadherin expression have been correlated with loss of cell-cell adhesion when proteolysis of the extracellular domain of cadherin generates peptides that disrupt the homotypic cadherin interaction on neighboring cells leading to invasion (47). The high levels of expression of proteases and low levels of expression of TIMPs in MTLn3 tumors are consistent with this possibility. In ovarian carcinoma cells of epithelial origin, cadherin expression promotes invasion, presumably by providing the adhesion and traction required for migration (48).

Collagen expression was lower, and collagen content, as measured by second harmonic generation, was significantly reduced in MTLn3 tumors. This latter observation is correlated with the higher levels of proteinase expression and lower levels of proteinase inhibitor expression in MTLn3 tumors compared with MTC tumors, suggesting significantly more proteolysis of ECM in MTLn3 tumors. These observations are consistent with the possibility of a large difference in signals for adhesion and motility in association with collagen fibers between MTLn3 and MTC tumors because proteolytic products of collagen are well known to stimulate adhesion and cell motility in culture (24). Chemotaxis to fragments of ECM has also been reported (4), suggesting that proteolysis in the local cell environment may elicit directional cell motility along ECM fibers as observed in MTLn3 tumors.

To invade, carcinoma cells need to penetrate through the basement membrane and remove ECM tissue boundaries (4). In this context, proteases are believed to play a key role because they can either degrade or process the ECM components and thereby support invasion and intravasation. The pattern of proteinase production and relative lack of proteinase inhibitors in MTLn3 tumors support the observed increase in invasion and intravasation in live animals.

Polarity and Chemotaxis of Carcinoma Cells toward Blood Vessels. One of the most remarkable observations made in live tumors both here and in previous studies was the dramatic polarization of carcinoma cells toward blood vessels in metastatic MTLn3 tumors (8). This was correlated with large differences in chemotaxis toward locally applied EGF in the primary tumor (25), increased blood burden of carcinoma cells in MTLn3 tumors as shown here, and metastatic efficiency (8), indicating that chemotaxis to blood vessels could increase the efficiency of intravasation and metastasis. Cell polarity and chemotaxis toward vessels could be induced by chemoattractant diffusing from the blood vessel. Growth factors including EGF, platelet-derived growth factor, FGF, and IGF are present in serum, macrophages, platelets, and smooth muscle cells associated with vessels (49–52). Release of growth factors from these cells or endothelial cells could provide a gradient that would produce a chemotactic response. Both our array data and results from other groups (40) demonstrate that MTLn3 cells express more EGFRs than MTC cells, and the data reported here show a significantly greater expression in MTLn3 tumors. However, MTC cells and tumors express much higher levels of FGF receptor and IGF-binding protein than MTLn3 cells and tumors. This suggests that chemotaxis toward vessels is specific to EGF because carcinoma cells in MTC tumors do not polarize and chemotax toward vessels. Experimental expression of the EGFR in MTC cells increases chemotactic responses to EGF *in vitro* and metastatic ability *in vivo* (9, 53, 54). Expression of the EGFR and its homologues, such as ErbB-2, has been correlated with poor prognosis in human breast tumors (55). Finally, chemotaxis to EGF has been demonstrated within MTLn3 primary tumors using microneedles containing Matrigel and EGF (25). Therefore, chemotaxis to blood vessels, mediated by the EGFR, is important in enhancing metastatic capability in addition to the well-characterized effects of EGFR signaling on mitogenesis.

Another positive correlation resulting from the comparison of cell behavior and expression analysis is the relationship between cell polarity and chemotaxis toward blood vessels. As reported previously (8, 12), metastatic primary tumors contain carcinoma cells that form loose clusters of rounded, nonpolarized cells except near blood vessels, where they are highly polarized toward vessels. Nonmetastatic primary tumors contain carcinoma cells with intrinsic polarity that are elongated and polarized in tight sheets regardless of the presence or absence of blood vessels. This was confirmed by examination of both the histopathology and intravital images of tumors (7, 8, 12, 25). Furthermore, the polarity of carcinoma cells in MTC tumors is closely correlated with the intrinsic polarity of the MTC cells in culture,

which exhibit polarized crawling, whereas MTLn3 cells do not exhibit intrinsic polarity and undergo random walking in culture (12).

A key difference between these cells that may explain the difference in intrinsic polarity is the targeting of mRNA for β-actin to the leading edge. In the array data reported here, MTC cells express much more ZBP-1, and this was confirmed at the protein level by Western blotting and immunohistochemistry. ZBP-1 is polarized at the cell pole in MTC cells in culture and in tumors, whereas it is diffuse in MTLn3 samples. This is correlated with the failure of MTLn3 cells to target β-actin mRNA to the leading edge and the failure to develop intrinsic polarity resulting in random walking (12). The mechanism relating mRNA targeting to the leading edge and intrinsic cell polarity involves the localization of β-actin nucleation to the leading edge during motility. Disruption of mRNA targeting to the leading edge using oligonucleotides that disrupt the interaction between ZBP-1 and the targeting sequence in the mRNA, the zipcode, results in delocalization of mRNA and β-actin nucleation sites and the disruption of cell polarity (56). The overexpression of ZBP-1 in MTC cells relative to MTLn3 cells is consistent with the higher level of intrinsic cell polarity of MTC cells in culture and in tumors. In general, cells that lack a fixed intrinsic polarity are more chemotactic to exogenous gradients presumably because there is no intrinsic polarity to be overcome by the exogenous chemotactic signal (12, 25, 56). This might explain why MTLn3 cells, with relatively low expression of ZBP-1 and no intrinsic polarity, were more polarized in a chemotactic field near blood vessels.

Cell Motility. A major difference between the motility of carcinoma cells in MTC and MTLn3 tumors is the local and nonlinear movement of cells in MTC tumors compared with the long linear excursions of carcinoma cells along collagen fibers and toward blood vessels seen in MTLn3 tumors. This is quite different from the motility of these cells in culture, where MTC cells exhibit linear crawling compared with the random walking of MTLn3 cells. This apparent reversal of behavior suggests that the motility of carcinoma cells in MTLn3 tumors is dominated by chemotaxis signals emanating from the processing of ECM and by chemoattractants associated with blood vessels. In addition, our array data suggest additional differences between MTC and MTLn3 cells in the expression of key proteins involved in leading edge dynamics that might contribute to enhanced chemotaxis ability.

Two functionally related proteins that are overexpressed in MTLn3 tumors and cells are the Arp2/3 complex and capping protein. The Arp2/3 complex is an EGFR-linked actin nucleation complex in the leading edge that nucleates actin filaments to elongate against the cell membrane to form lamellipods (33, 57). This event determines cell polarity in response to EGF stimulation and is a key first step in chemotaxis (24, 33). The greatly increased expression of Arp2/3 complex in MTLn3 cells is expected to significantly enhance chemotaxis of carcinoma cells in MTLn3 tumors and in culture because inhibition of the nucleation activity of Arp2/3 complex in carcinoma cells inhibits chemotaxis to EGF (33). In addition, the higher expression of capping protein in MTLn3 tumors is expected to greatly enhance the efficiency of nucleation by Arp2/3 complex (34).

A functionally related protein that is overexpressed in MTC cells and tumors is cortactin. Cortactin is tyrosine phosphorylated in response to FGF and EGF in fibroblasts (58) (59) and binds to Arp2/3 complex and stimulates its nucleation activity weakly but strongly stabilizes Arp2/3-mediated filament branches (36). The relative overexpression of cortactin in MTC cells and tumors reported here is consistent with the higher level of intrinsic polarity of carcinoma cells in MTC tumors and in culture, where the stabilizing effect of cortactin on the actin network at the leading edge could stabilize cell polarity.

Mechanical Stability and Survival during Intravasation. The majority of tumor cells that enter the circulation are rapidly eliminated by the immune system or apoptosis. Fibrin deposits, platelet aggregation, and cell adhesion in tumor emboli may protect circulating cells from mechanical trauma, facilitate their arrest in capillary beds, and protect tumor emboli from destruction by host immunity (60). From our array data, we have found that carcinoma cells in MTLn3 tumors and culture highly express laminins and cadherins and apoptosis suppressor genes, all of which may contribute to survival in the circulation. In contrast, carcinoma cells in MTC tumors and culture express genes involved in programmed cell death at higher levels. The combination of these factors may contribute to the increased numbers of viable carcinoma cells in the circulation of MTLn3 tumors.

A novel observation resulting from intravital imaging of these tumors is the dramatic fragmentation of carcinoma cells when in contact with blood vessels in MTC tumors (8) compared with the ability of carcinoma cells in MTLn3 tumors to enter blood vessels as intact whole cells as shown here. A potential explanation for this difference in behavior is the large relative overexpression of cytokeratins by carcinoma cells in MTLn3 tumors. These keratins form the largest subfamily of intermediate filament proteins and play critical roles in the mechanical stability of epithelial cells subjected to shear forces (61).

In conclusion, we have developed animal models of breast cancer that allow the direct examination of the behavior of individual GFP-expressing carcinoma cells in live nonmetastatic and metastatic primary tumors *in situ*. When combined with multiphoton microscopy to image differences in cell behavior, insights into the microenvironment of carcinoma cells in the primary tumor can be obtained. When correlated with results from cDNA microarray analyses, the behavioral insights allow the identification of potentially important genetic determinants for breast cancer invasion and metastasis. We conclude that aligning cell behavior *in vivo* with patterns of gene expression can lead to the molecular mechanisms behind invasion and metastasis.

ACKNOWLEDGMENTS

We gratefully acknowledge Dr. Jeffrey W. Pollard for critical reading and valuable discussion of the manuscript. We also thank Dr. Weijia Zhang for help with microarray analysis. We are grateful to Aldo Massimi (AECOM Microarray Core) and members of the Analytical Imaging Facility for support and advice. We thank Dr. Mariana Dabeva of the AECOM Liver Center for advice about using mouse cDNA arrays.

REFERENCES

1. Fidler, I. J. Critical determinants of cancer metastasis: rationale for therapy. Cancer Chemother. Pharmacol., *43:* S3–S10, 1999.
2. Morris, V. L., Schmidt, E. E., MacDonald, I. C., Groom, A. C., and Chambers, A. F. Sequential steps in hematogenous metastasis of cancer cells studied by *in vivo* videomicroscopy. Invasion Metastasis, *17:* 281–296, 1997.
3. Naumov, G. N., Wilson, S. M., MacDonald, I. C., Schmidt, E. E., Morris, V. L., Groom, A. C., Hoffman, R. M., and Chambers, A. F. Cellular expression of green fluorescent protein, coupled with high-resolution *in vivo* videomicroscopy, to monitor steps in tumor metastasis. J. Cell Sci., *112:* 1835–1842, 1999.
4. Liotta, L. A., and Kohn, E. C. The microenvironment of the tumour-host interface. Nature (Lond.), *411:* 375–379, 2001.
5. Perou, C. M., Sorlie, T., Eisen, M. B., van de Rijn, M., Jeffrey, S. S., Rees, C. A., Pollack, J. R., Ross, D. T., Johnsen, H., Akslen, L. A., Fluge, O., Pergamenschikov, A., Williams, C., Zhu, S. X., Lonning, P. E., Borresen-Dale, A. L., Brown, P. O., and Botstein, D. Molecular portraits of human breast tumours. Nature (Lond.), *406:* 747–752, 2000.
6. Bonner, R. F., Emmert-Buck, M., Cole, K., Pohida, T., Chuaqui, R., Goldstein, S., and Liotta, L. A. Laser capture microdissection: molecular analysis of tissue. Science (Wash. DC), *278:* 1481, 1483, 1997.
7. Farina, K. L., Wyckoff, J. B., Rivera, J., Lee, H., Segall, J. E., Condeelis, J. S., and Jones, J. G. Cell motility of tumor cells visualized in living intact primary tumors using green fluorescent protein. Cancer Res., *58:* 2528–2532, 1998.
8. Wyckoff, J. B., Jones, J. G., Condeelis, J. S., and Segall, J. E. A critical step in metastasis: *in vivo* analysis of intravasation at the primary tumor. Cancer Res., *60:* 2504–2511, 2000.

9. Wyckoff, J. B., Insel, L., Khazaie, K., Lichtner, R. B., Condeelis, J. S., and Segall, J. E. Suppression of ruffling by the EGF receptor in chemotactic cells. Exp. Cell Res., *242:* 100–109, 1998.
10. Neri, A., Welch, D., Kawaguchi, T., and Nicolson, G. L. Development and biologic properties of malignant cell sublines and clones of a spontaneously metastasizing rat mammary adenocarcinoma. J. Natl. Cancer Inst. (Bethesda), *68:* 507–517, 1982.
11. Edmonds, B. T., Bell, A., Wyckoff, J., Condeelis, J., and Leyh, T. S. The effect of F-actin on the binding and hydrolysis of guanine nucleotide by *Dictyostelium* elongation factor 1A. J. Biol. Chem., *273:* 10288–10295, 1998.
12. Shestakova, E. A., Wyckoff, J., Jones, J., Singer, R. H., and Condeelis, J. Correlation of β-actin messenger RNA localization with metastatic potential in rat adenocarcinoma cell lines. Cancer Res., *59:* 1202–1205, 1999.
13. Centonze, V. E., and White, J. G. Multiphoton excitation provides optical sections from deeper within scattering specimens than confocal imaging. Biophys. J., *75:* 2015–2024, 1998.
14. Williams, R. M., Zipfel, W. R., and Webb, W. W. Multiphoton microscopy in biological research. Curr. Opin. Chem. Biol., *5:* 603–608, 2001.
15. Soll, D. R. The use of computers in understanding how animal cells crawl. Int. Rev. Cytol., *163:* 43–104, 1995.
16. Cheung, V. G., Morley, M., Aguilar, F., Massimi, A., Kucherlapati, R., and Childs, G. Making and reading microarrays. Nat. Genet., *21:* 15–19, 1999.
17. Zavadil, J., Bitzer, M., Liang, D., Yang, Y. C., Massimi, A., Kneitz, S., Piek, E., and Bottinger, E. P. Genetic programs of epithelial cell plasticity directed by transforming growth factor-β. Proc. Natl. Acad. Sci. USA, *98:* 6686–6691, 2001.
18. Chauhan, B. K., Reed, N. A., Zhang, W., Duncan, M. K., Kilimann, M. W., and Cvekl, A. Identification of genes downstream of Pax6 in the mouse lens using cDNA microarrays. J. Biol. Chem., *277:* 11539–11548, 2002.
19. Ross, A. F., Oleynikov, Y., Kislauskis, E. H., Taneja, K. L., and Singer, R. H. Characterization of a β-actin mRNA zipcode-binding protein. Mol. Cell. Biol., *17:* 2158–2165, 1997.
20. Edmonds, B. T., Wyckoff, J., Yeung, Y. G., Wang, Y., Stanley, E. R., Jones, J., Segall, J., and Condeelis, J. Elongation factor-1 α is an overexpressed actin binding protein in metastatic rat mammary adenocarcinoma. J. Cell Sci., *109:* 2705–2714, 1996.
21. Welch, M. D., DePace, A. H., Verma, S., Iwamatsu, A., and Mitchison, T. J. The human Arp2/3 complex is composed of evolutionarily conserved subunits and is localized to cellular regions of dynamic actin filament assembly. J. Cell Biol., *138:* 375–384, 1997.
22. Denk, W., Strickler, J. H., and Webb, W. W. Two-photon laser scanning fluorescence microscopy. Science (Wash. DC), *248:* 73–76, 1990.
23. Campagnola, P. J., Clark, H. A., Mohler, W. A., Lewis, A., and Loew, L. M. Second-harmonic imaging microscopy of living cells. J. Biomed. Opt., *6:* 277–286, 2001.
24. Bailly, M., Yan, L., Whitesides, G. M., Condeelis, J. S., and Segall, J. E. Regulation of protrusion shape and adhesion to the substratum during chemotactic responses of mammalian carcinoma cells. Exp. Cell Res., *241:* 285–299, 1998.
25. Wyckoff, J. B., Segall, J. E., and Condeelis, J. S. The collection of the motile population of cells from a living tumor. Cancer Res., *60:* 5401–5404, 2000.
26. Dong, G., Loukinova, E., Chen, Z., Gangi, L., Chanturita, T. I., Liu, E. T., and Van Waes, C. Molecular profiling of transformed and metastatic murine squamous carcinoma cells by differential display and cDNA microarray reveals altered expression of multiple genes related to growth, apoptosis, angiogenesis, and the NF-κB signal pathway. Cancer Res., *61:* 4797–4808, 2001.
27. Doyle, G. A., Betz, N. A., Leeds, P. F., Fleisig, A. J., Prokipcak, R. D., and Ross, J. The c-myc coding region determinant-binding protein: a member of a family of KH domain RNA-binding proteins. Nucleic Acids Res., *26:* 5036–5044, 1998.
28. Ross, J., Lemm, I., and Berberet, B. Overexpression of an mRNA-binding protein in human colorectal cancer. Oncogene, *20:* 6544–6550, 2001.
29. Zhang, J. Y., Chan, E. K., Peng, X. X., and Tan, E. M. A novel cytoplasmic protein with RNA-binding motifs is an autoantigen in human hepatocellular carcinoma. J. Exp. Med., *189:* 1101–1110, 1999.
30. Jesaitis, L. A., and Goodenough, D. A. Molecular characterization and tissue distribution of ZO-2, a tight junction protein homologous to ZO-1 and the *Drosophila* discs-large tumor suppressor protein. J. Cell Biol., *124:* 949–961, 1994.
31. Fitter, S., Sincock, P. M., Jolliffe, C. N., and Ashman, L. K. Transmembrane 4 superfamily protein CD151 (PETA-3) associates with β_1 and $\alpha_{IIb}\beta_3$ integrins in haemopoietic cell lines and modulates cell-cell adhesion. Biochem. J., *338:* 61–70, 1999.
32. Wei, P., Zhao, Y. G., Zhuang, L., Ruben, S., and Sang, Q. X. Expression and enzymatic activity of human disintegrin and metalloproteinase ADAM19/meltrin β. Biochem. Biophys. Res. Commun., *280:* 744–755, 2001.
33. Bailly, M., Ichetovkin, I., Grant, W., Zebda, N., Machesky, L. M., Segall, J. E., and Condeelis, J. The F-actin side binding activity of the Arp2/3 complex is essential for actin nucleation and lamellipod extension. Curr. Biol., *11:* 620–625, 2001.
34. Carlier, M. F. Control of actin dynamics. Curr. Opin. Cell Biol., *10:* 45–51, 1998.
35. Takaishi, K., Matozaki, T., Nakano, K., and Takai, Y. Multiple downstream signalling pathways from ROCK, a target molecule of Rho small G protein, in reorganization of the actin cytoskeleton in Madin-Darby canine kidney cells. Genes Cells, *5:* 929–936, 2000.
36. Weaver, A. M., Karginov, A. V., Kinley, A. W., Weed, S. A., Li, Y., Parsons, J. T., and Cooper, J. A. Cortactin promotes and stabilizes Arp2/3-induced actin filament network formation. Curr. Biol., *11:* 370–374, 2001.
37. Huang, P., and Oliff, A. Signaling pathways in apoptosis as potential targets for cancer therapy. Trends Cell Biol., *11:* 343–348, 2001.
38. Marion, R. M., Fortes, P., Beloso, A., Dotti, C., and Ortin, J. A human sequence homologue of Staufen is an RNA-binding protein that is associated with polysomes and localizes to the rough endoplasmic reticulum. Mol. Cell. Biol., 19: 2212–2219, 1999.
39. Liu, G., Grant, W. M., Persky, D., Latham, V. M., Jr., Singer, R. H., and Condeelis, J. Interactions of elongation factor 1α with F-actin and β-actin mRNA: implications for anchoring mRNA in cell protrusions. Mol. Biol. Cell, *13:* 579–592, 2002.
40. Kaufmann, A. M., Khazaie, K., Wiedemuth, M., Rohde-Schulz, B., Ullrich, A., Schirrmacher, V., and Lichtner, R. B. Expression of epidermal growth factor receptor correlates with metastatic potential of 13762NF rat mammary adenocarcinoma cells. Int. J. Oncol., *4:* 1149–1155, 1994.
41. Lanzetti, L., Rybin, V., Malabarba, M. G., Christoforidis, S., Scita, G., Zerial, M., and Di Fiore, P. P. The Eps8 protein coordinates EGF receptor signalling through Rac and trafficking through Rab5. Nature (Lond.), *408:* 374–377, 2000.
42. Zhang, W., Razani, B., Altschuler, Y., Bouzahzah, B., Mostov, K. E., Pestell, R. G., and Lisanti, M. P. Caveolin-1 inhibits epidermal growth factor-stimulated lamellipod extension and cell migration in metastatic mammary adenocarcinoma cells (MTLn3). Transformation suppressor effects of adenovirus-mediated gene delivery of caveolin-1. J. Biol. Chem., *275:* 20717–20725, 2000.
43. Sanders, L. C., Matsumura, F., Bokoch, G. M., and de Lanerolle, P. Inhibition of myosin light chain kinase by p21-activated kinase. Science (Wash. DC), *283:* 2083–2085, 1999.
44. Wozney, J. M., Rosen, V., Celeste, A. J., Mitsock, L. M., Whitters, M. J., Kriz, R. W., Hewick, R. M., and Wang, E. A. Novel regulators of bone formation: molecular clones and activities. Science (Wash. DC), *242:* 1528–1534, 1988.
45. Kessler, E., Takahara, K., Biniaminov, L., Brusel, M., and Greenspan, D. S. Bone morphogenetic protein-1: the type I procollagen C-proteinase. Science (Wash. DC), *271:* 360–362, 1996.
46. Sommers, C. L. The role of cadherin-mediated adhesion in breast cancer. J. Mammary Gland Biol. Neoplasia, *1:* 219–229, 1996.
47. Noe, V., Chastre, E., Bruyneel, E., Gespach, C., and Mareel, M. Extracellular regulation of cancer invasion: the E-cadherin-catenin and other pathways. Biochem. Soc. Symp., *65:* 43–62, 1999.
48. Ong, A., Maines-Bandiera, S. L., Roskelley, C. D., and Auersperg, N. An ovarian adenocarcinoma line derived from SV40/E-cadherin-transfected normal human ovarian surface epithelium. Int. J. Cancer, *85:* 430–437, 2000.
49. Calabro, A., Orsini, B., Renzi, D., Papi, L., Surrenti, E., Amorosi, A., Herbst, H., Milani, S., and Surrenti, C. Expression of epidermal growth factor, transforming growth factor-α and their receptor in the human oesophagus. Histochem. J., *29:* 745–758, 1997.
50. Peoples, G. E., Blotnick, S., Takahashi, K., Freeman, M. R., Klagsbrun, M., and Eberlein, T. J. T lymphocytes that infiltrate tumors and atherosclerotic plaques produce heparin-binding epidermal growth factor-like growth factor and basic fibroblast growth factor: a potential pathologic role. Proc. Natl. Acad. Sci. USA, *92:* 6547–6551, 1995.
51. Kume, N., and Gimbrone, M. A., Jr. Lysophosphatidylcholine transcriptionally induces growth factor gene expression in cultured human endothelial cells. J. Clin. Invest., *93:* 907–911, 1994.
52. Dluz, S. M., Higashiyama, S., Damm, D., Abraham, J. A., and Klagsbrun, M. Heparin-binding epidermal growth factor-like growth factor expression in cultured fetal human vascular smooth muscle cells. Induction of mRNA levels and secretion of active mitogen. J. Biol. Chem., *268:* 18330–18334, 1993.
53. Lichtner, R. B., Kaufmann, A. M., Kittmann, A., Rohde-Schulz, B., Walter, J., Williams, L., Ullrich, A., Schirrmacher, V., and Khazaie, K. Ligand mediated activation of ectopic EGF receptor promotes matrix protein adhesion and lung colonization of rat mammary adenocarcinoma cells. Oncogene, *10:* 1823–1832, 1995.
54. Kaufmann, A. M., Lichtner, R. B., Schirrmacher, V., and Khazaie, K. Induction of apoptosis by EGF receptor in rat mammary adenocarcinoma cells coincides with enhanced spontaneous tumour metastasis. Oncogene, *13:* 2349–2358, 1996.
55. Henderson, I. C., and Patek, A. J. The relationship between prognostic and predictive factors in the management of breast cancer. Breast Cancer Res. Treat., *52:* 261–288, 1998.
56. Shestakova, E. A., Singer, R. H., and Condeelis, J. The physiological significance of β-actin mRNA localization in determining cell polarity and directional motility. Proc. Natl. Acad. Sci. USA, *98:* 7045–7050, 2001.
57. Cooper, J. A., Wear, M. A., and Weaver, A. M. Arp2/3 complex: advances on the inner workings of a molecular machine. Cell, *107:* 703–705, 2001.
58. Maa, M. C., Wilson, L. K., Moyers, J. S., Vines, R. R., Parsons, J. T., and Parsons, S. J. Identification and characterization of a cytoskeleton-associated, epidermal growth factor sensitive pp60c-src substrate. Oncogene, *7:* 2429–2438, 1992.
59. Weed, S. A., and Parsons, J. T. Cortactin: coupling membrane dynamics to cortical actin assembly. Oncogene, *20:* 6418–6434, 2001.
60. Fournier, M. V., Carvalho, M. G., and Pardee, A. B. A strategy to identify genes associated with circulating solid tumor cell survival in peripheral blood. Mol. Med., *5:* 313–319, 1999.
61. Coulombe, P. A., and Omary, M. B. "Hard" and "soft" principles defining the structure, function and regulation of keratin intermediate filaments. Curr. Opin. Cell Biol., *14:* 110–122, 2002.